# MURDOCH RESEARCH REPOSITORY

*This is the author's final version of the work, as accepted for publication following peer review but without the publisher's layout or pagination.*

**Forbes, L.K. and Hocking, G.C. (2010) Unsteady draining of a fluid from a circular tank. Applied Mathematical Modelling, 34 (12). pp. 3958-3975.**

# Accepted Manuscript

Unsteady Draining of a Fluid from a Circular Tank

Lawrence K. Forbes, Graeme C. Hocking

Please cite this article as: L.K. Forbes, G.C. Hocking, Unsteady Draining of a Fluid from a Circular Tank, *Appl. Math. Modelling* (2010), doi: 10.1016/j.apm.2010.03.032
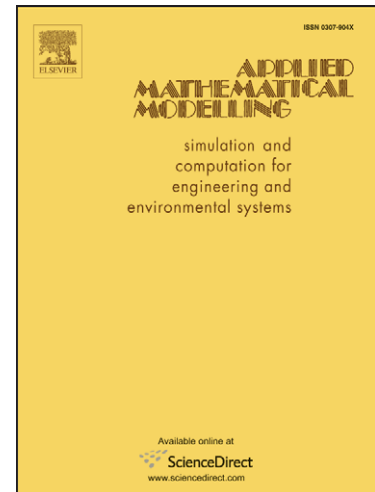
# Unsteady Draining of a Fluid
# from a Circular Tank

Lawrence K. Forbes
School of Mathematics and Physics,
University of Tasmania,
Hobart 7001, Tasmania, Australia.
mailto:Larry.Forbes@utas.edu.au

Graeme C. Hocking
School of Mathematics and Statistics,
Division of Science, Murdoch University,
Murdoch 6150, Western Australia, Australia.

## Abstract

Three-dimensional draining flow of a two-fluid system from a circular tank is considered. The two fluids are inviscid and incompressible, and are separated by a sharp interface. There is a circular hole positioned centrally in the bottom of the tank, so that the flow is axially symmetric. The mean position of the interface moves downwards as time progresses, and eventually a portion of the interface is withdrawn into the drain. For narrow drain holes of small radius, the interface above the centre of the drain is pulled down towards the hole. However, for drains of larger radius the portion of the interface above the drain edge is drawn down first, rather than the central section. Nonlinear results are obtained with a novel spectral technique, and are also compared against the predictions of linearized theory. Unstable Rayleigh-Taylor type flows, in which the upper fluid is heavier than the lower one, are also discussed.

1

# 1    Introduction

In recent years, there has been much work undertaken on the extraction of fluid from reservoirs. In the simplest version of the problem, the extraction sink can be idealized to be a mathematical point sink (or a line sink for two-dimensional flow), and the fluid can be considered to be infinitely deep. If, in addition, the fluid is assumed to be ideal, in the sense that it is incompressible and inviscid, then the problem has a particularly simple formulation, and may rightly be regarded as one of the canonical problems in non-linear free-surface hydrodynamics. A velocity potential function $\phi$ exists in the fluid, and the velocity can be calculated simply by taking its gradient. The governing equation in the fluid is then Laplace's equation, but there are non-linear conditions to be satisfied on the moveable fluid interface, the location of which is unknown in advance.

This problem is of importance in the practical operation of extraction pumps in reservoirs, for example. This is because, for unbounded fluid, there is a maximum value of the extraction rate (volume per time) at which fluid can be removed. As the pumping rate is increased, the free surface of the fluid is pulled down towards the pump, and at the maximum extraction rate, the surface is drawn right into the pump itself. From an operational point of view, this then defines the maximum extraction rate for continuous, steady-state withdrawal from a single layer of fluid. There have been a number of experiments aimed at determining this upper limit, and some of these are summarized by Jirka and Katavola [1]. This general class of withdrawal flows has even been suggested to have a potential use in the coating of microparticles, as indicated by Cohen *et al* [2].

For steady, two-dimensional flow, an early theoretical investigation was undertaken by Peregrine [3]. A later study by Tuck and Vanden-Broeck [4] then showed that there are two types of steady solution, one valid for a range of low extraction rates and a second type at a unique higher value. This second type has the free surface just at the point of being drawn into the sink in a vertical cusp, and was seen as possibly corresponding to the maximum extraction rate for steady-state operation. It is now known that the situation is rather more complicated than this. In particular, Stokes *et al* [5] showed numerically that there is a complicated relationship between steady-state and unsteady solutions, and the critical extraction rate that divides one solution type from another may depend sensitively on the initial conditions for the flow. Forbes *et al* [6] used linearized theory and stationary-phase arguments to study the effect of initial conditions on two-dimensional and three-dimensional extraction flows. Nevertheless, much of the complexity of the unsteady solution behaviour is not available to the linearized approx-

imation, and numerical methods are also needed in solutions of the fully non-linear problem.

Three-dimensional flows into point extraction sinks have also received much attention. For steady-state flows, there is again a maximum extraction rate, beyond which presumably only transient unsteady flow types are possible. Forbes and Hocking [7] used an integral-equation method to compute steady-state flows into a sink in an unbounded fluid with an otherwise horizontal surface, and found that the maximum steady extraction rate is characterized by the formation of a circular ring of stagnation points at the free surface. A similar, but geometrically more complex, situation was encountered by Forbes and Hocking [8] when considering the effect of a nearby vertical reservoir wall.

Unsteady flows into point sinks in three dimensional geometry have also been studied, and likewise show a complex relationship between the transient solutions and the steady-state ones. An earlier investigation was carried out by Miloh and Tyvand [9], who used low-order Taylor series expansions in time to estimate the critical time at which the free surface might be pulled down into the sink. A similar analysis was also undertaken by Haugen and Tyvand [10]. Later, Xue and Yue [11] carried out a numerical investigation into the unsteady flow caused by an impulsively started point sink in a fluid, and found three different types of flow behaviour, depending on the strength of the sink. There could be an evolution toward an eventual steady-state flow for weak sinks, but for stronger sinks the unsteady flow might involve an upwardly-directed jet at the surface, or else the direct withdrawal of the surface into the sink. These findings have been confirmed by Stokes *et al* [5], [12].

Axially symmetric flow into a hole at the bottom of a cylindrical tank was investigated numerically by Zhou and Graebel [13] for potential flows. They considered both the draining of a single fluid layer as well as a two-fluid system with a sharp interface between the two fluid layers, and used an integral-equation method to compute the location of the surface or interface. They found that the behaviour of the solution was dependent upon the strength of the sink on the tank bottom and its radius. Similarly to the work of Xue and Yue [11] for a point sink, there could be solutions in which the interface either was drawn right into the sink, or else formed an upwardly-directed jet at the centre of the tank. However, unlike the case of the point sink in an unbounded fluid, there is no option here for the flow to reach a steady state, since the tank is draining continuously.

Very similar results to those of Zhou and Graebel [13] have been obtained by Baek and Chung [14], in a numerical solution of the Navier-Stokes equations for incompressible viscous fluid. This suggests that viscous effects may

3

therefore not have a major influence on most of the details of the flow. This was confirmed in recent numerical work of Farrow and Hocking [15], for two-dimensional draining flows in a rectangular tank. The fully inviscid version of this two-dimensional flow was studied by Forbes and Hocking [16] using a time-dependent spectral method, and they showed that they were able to reproduce the Farrow and Hocking [15] solutions very closely, adding weight to the suggestion that viscosity and interface thickness might normally only play a minor role in the overall draining flow. Nevertheless, Forbes and Hocking [16] observed that regions of very high curvature could form at the interface within finite time, and this raises the possibility that viscosity could then trigger roll-up at certain points along the interface, towards the end of the draining process.

In the present paper, we investigate the axially symmetric draining flow of a three dimensional circular tank. This is essentially the problem studied by Zhou and Graebel [13]. Here, however, we use an extended version of the novel spectral method developed by Forbes *et al* [17]. This is a similar technique to that used by Kim *et al* [18], in that the solution to Laplace's equation in each fluid layer is used explicitly. However, the method uses identities derived from the conditions along the interface, and integration by parts, to obtain a compact set of ordinary differential equations for the (time-dependent) Fourier coefficients. These are integrated numerically using a Runge-Kutta method. In addition, the interface may be represented parametrically in terms of a scaled arclength variable, and this allows interface overturning to be followed, if it should occur. This same technique was used by Forbes and Hocking [16] in their study of planar withdrawal from a tank.

The governing equations are briefly reviewed in section 2 for the axially symmetric withdrawal problem, and the linearized solution is then presented in section 3. The solution algorithm for the fully non-linear equations is developed in section 4. It extends the planar method of Forbes and Hocking [16] to axially symmetric geometry, making use of identities for the first-kind Bessel functions that are necessary to represent the solution. The non-linear results are presented in sections 5 and 6, and although the case of most practical interest is when fluid is draining through the hole in the bottom of the tank, we have also considered the possibility that the hole may act as a source, through which fluid is injected into the lower fluid layer. This is easily accommodated into the present numerical scheme, simply by allowing the drain strength to be negative. It is found that the linearized approximation gives a good description of the flow for most parameter values, although non-linear effects suddenly become dominant when the interface drains down close to the bottom of the tank. The time required to drain the lower fluid layer

4

from the tank is therefore significantly influenced by non-linear effects. A discussion of these results is given in section 7, along with some concluding remarks.

# 2   Mathematical Formulation

Consider a circular cylindrical tank of radius $W$ and height $H + L$. A cartesian coordinate system is located such that the $x$-$y$ plane lies along the tank bottom, with the $z$-axis pointing vertically up the centre axis of the cylindrical tank. At time $t = 0$, there is a fluid of density $\rho_1$ in $0 < z < H$ and a second fluid of density $\rho_2$ in the volume $H < z < H + L$, following the notation in Batchelor ([19], page 69). Each fluid is ideal, in the sense that it is incompressible and inviscid, and there is a sharp interface separating them. At time $t = 0$, this interface is located on the plane $z = H$. Each fluid is subject to the downward acceleration $g$ of gravity.

A drain hole of radius $A$ is present on the tank bottom, and is positioned symmetrically with its centre lying on the $z$-axis. The sink at the bottom is turned on impulsively at time $t = 0$, so that it withdraws fluid from lower layer 1 at the constant volume flow rate $Q$ for all times $t > 0$. As a consequence, the interface between the fluids moves downwards toward the bottom of the tank, and its shape changes with time. Mathematically, it is represented by the surface $z = \eta(x, y, t)$. Eventually, some portion of the interface is pulled into the drain hole, and the mathematical model then ceases to be valid.

For simplicity, it is assumed that the vertical component of the fluid velocity vector is constant at the drain, and by conservation of mass in the lower fluid layer, the withdrawal speed at the hole must therefore be $-Q/(\pi A^2 \rho_1)$. Upper fluid 2 must be re-charged at the same volume flow rate (since each fluid is incompressible). It is assumed that there is a constant re-charge speed everywhere over the top of the tank, so that the vertical component of velocity of the upper fluid is $-Q/(\pi W^2 \rho_1)$ on the plane $z = H + L$.

In view of the axial symmetry of the problem, it is appropriate now to transform into cylindrical polar coordinates $(r, \theta, z)$, using the usual relations $x = r \cos \theta$ and $y = r \sin \theta$. Thus the interface is represented in the form $z = \eta(r, t)$.

For convenience, non-dimensional variables are introduced, and these will be assumed throughout the rest of this paper. All lengths are scaled with respect to the initial interface height $H$ and times are referenced to the quantity $\sqrt{H/g}$. The unit of speed is therefore $\sqrt{gH}$. The dimensionless
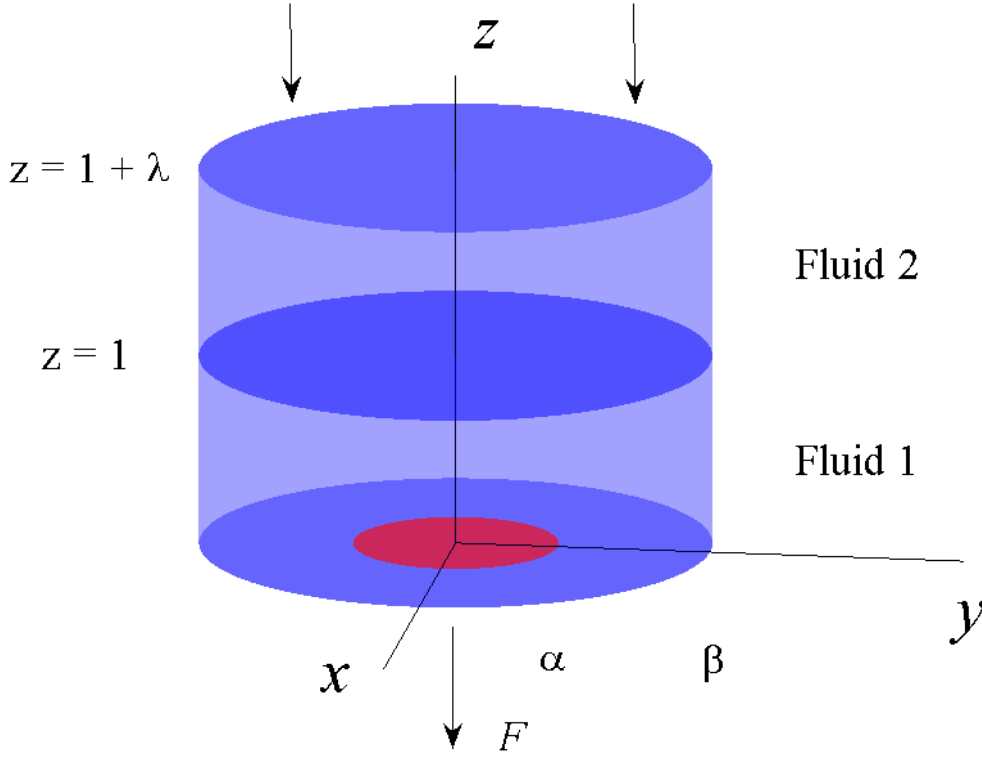
5

Figure 1: An illustration of the non-dimensional flow geometry for axially symmetric withdrawal from a two-fluid system in a cylindrical tank.

problem thus involves the five parameters

$$F = Q/\left(\rho_1\sqrt{gH^5}\right) \qquad \alpha = A/H \qquad \beta = W/H$$
$$\lambda = L/H \qquad D = \rho_2/\rho_1 \qquad (2.1)$$

and these are assumed to be constants. The first of these, $F$, is a Froude number and represents the dimensionless mass extraction rate through the drain hole. Constants $\alpha$ and $\beta$ are respectively the radius of the hole in the bottom of the tank and the radius of the tank itself. The height of the tank is $1+\lambda$ and $D$ is the density ratio of the two fluids. In these non-dimensional variables, the initial interface height is therefore $\eta = 1$. This flow situation is illustrated in Figure 1.

Each fluid is incompressible and inviscid, and therefore flows irrotationally. Accordingly, velocity potentials $\phi_1$ and $\phi_2$ can be constructed in each fluid layer, such that the fluid velocities can be obtained from the gradients

6

of each function. In cylindrical polar coordinates and axially symmetric flow, the velocities are $u_i\mathbf{e_r} + w_i\mathbf{e_z}$ with components $u_i$ and $w_i$ in the radial $\mathbf{e_r}$ and axial $\mathbf{e_z}$ directions, respectively, $i = 1, 2$, and so it follows that $u_i = \partial\phi_i/\partial r$ and $w_i = \partial\phi_i/\partial z$, $i = 1, 2$. Each velocity potential satisfies Laplace's equation, so that

$$\frac{\partial^2\phi_1}{\partial r^2} + \frac{1}{r}\frac{\partial\phi_1}{\partial r} + \frac{\partial^2\phi_1}{\partial z^2} = 0 \quad \text{in } 0 < z < \eta(r,t) \tag{2.2}$$

and

$$\frac{\partial^2\phi_2}{\partial r^2} + \frac{1}{r}\frac{\partial\phi_2}{\partial r} + \frac{\partial^2\phi_2}{\partial z^2} = 0 \quad \text{in } \eta(r,t) < z < 1 + \lambda. \tag{2.3}$$

On the tank bottom, the vertical component of fluid velocity in the lower layer satisfies

$$w_1 = \begin{cases} -F/\left(\pi\alpha^2\right) & \text{if } 0 < r < \alpha \\ 0 & \text{if } \alpha < r < \beta \end{cases} \tag{2.4}$$

There is no flow through the side walls of the tank, so that the boundary conditions there are simply

$$u_i = 0 \quad \text{on } r = \beta, \quad i = 1, 2. \tag{2.5}$$

As fluid drains from the bottom of the tank, it must be re-charged at the same volume flow rate at the top (since each fluid is incompressible). Therefore

$$w_2 = -F/\left(\pi\beta^2\right) \quad \text{on } z = 1 + \lambda. \tag{2.6}$$

It is also necessary to impose boundary conditions on the moving interface $z = \eta(r,t)$ itself. There are kinematic requirements on the fluid on either side, which may be expressed in the form

$$w_i = \frac{\partial\eta}{\partial t} + u_i\frac{\partial\eta}{\partial r}, \quad i = 1, 2 \quad \text{on } z = \eta \tag{2.7}$$

and these represent the fact that neither fluid may cross the interface. Since each fluid is ideal, the equations of motion may be integrated to give Bernoulli equations relating the pressures and speeds in each fluid; equating the pressures at the interface then yields the dynamic condition

$$D\frac{\partial\phi_2}{\partial t} - \frac{\partial\phi_1}{\partial t} + \tfrac{1}{2}D\left(u_2^2 + w_2^2\right) - \tfrac{1}{2}\left(u_1^2 + w_1^2\right) + (D-1)\eta$$
$$= \tfrac{1}{2}(D-1)\frac{F^2}{\pi^2\beta^4} + (D-1)\left(1 - \frac{Ft}{\pi\beta^2}\right) \quad \text{on } z = \eta. \tag{2.8}$$

7

Following Forbes and Hocking [16], the steady-state solution $\phi^S(r, z)$ to the equations (2.2)–(2.8) is subtracted from the potentials $\phi_1$ and $\phi_2$. This is expressed by means of the equations

$$\phi_i(r, z, t) = \phi^S(r, z) + \Phi_i(r, z, t), \quad i = 1, 2, \tag{2.9}$$

and the intention is now to solve for the perturbation potentials $\Phi_1$ and $\Phi_2$ that contain information about the time-dependent behaviour. The solution for the steady-state potential $\phi^S(r, z)$ in equations (2.9) is obtained using separation of variables techniques, and after some algebra gives a Fourier-Bessel series of the form

$$\phi^S(r, z) = -\frac{Fz}{\pi\beta^2} + \sum_{n=1}^{\infty} P_n^S J_0\left(j_{1,n}\frac{r}{\beta}\right) \cosh\left(\frac{j_{1,n}}{\beta}(1 + \lambda - z)\right). \tag{2.10}$$

The coefficients $P_n^S$ in this expression are obtained by making equation (2.10) satisfy the bottom condition (2.4). After using the orthogonality conditions and recurrence relations for Bessel functions, given in Abramowitz and Stegun [20], it is possible to derive the explicit expression

$$P_n^S = \frac{2F J_1\big(j_{1,n}\alpha/\beta\big)}{\pi\alpha \sinh\big(j_{1,n}(1 + \lambda)/\beta\big)\big(j_{1,n}\big)^2 J_0^2\big(j_{1,n}\big)}. \tag{2.11}$$

For later reference, we also record the radial and axial velocity components derived from this steady-state solution (2.10). These are

$$u^S(r, z) = -\sum_{n=1}^{\infty} \frac{j_{1,n}}{\beta} P_n^S J_1\left(j_{1,n}\frac{r}{\beta}\right) \cosh\left(\frac{j_{1,n}}{\beta}(1 + \lambda - z)\right)$$

$$w^S(r, z) = -\frac{F}{\pi\beta^2}$$

$$- \sum_{n=1}^{\infty} \frac{j_{1,n}}{\beta} P_n^S J_0\left(j_{1,n}\frac{r}{\beta}\right) \sinh\left(\frac{j_{1,n}}{\beta}(1 + \lambda - z)\right). \tag{2.12}$$

The constant $j_{1,n}$ in equations (2.10)–(2.12) is the $n$-th zero of the $J_1$ Bessel function.

The governing equations (2.2)–(2.8) are now re-written in terms of the new perturbed potentials $\Phi_1$ and $\Phi_2$ introduced in equation (2.9). These potentials obey Laplace's equations (2.2) and (2.3) in fluids 1 and 2. The bottom condition (2.4) becomes simply

$$\partial\Phi_1/\partial z = 0 \quad \text{on } z = 0 \tag{2.13}$$

8

and the top condition (2.6) becomes

$$\partial\Phi_2/\partial z = 0 \quad \text{on } z = 1 + \lambda. \tag{2.14}$$

At the sides of the tank, the perturbed potentials also obey the condition (2.5). The kinematic interfacial conditions (2.7) now become

$$\left(w^S + \frac{\partial\Phi_i}{\partial z}\right) = \frac{\partial\eta}{\partial t} + \left(u^S + \frac{\partial\Phi_i}{\partial r}\right)\frac{\partial\eta}{\partial r}, \quad i = 1, 2 \quad \text{on } z = \eta \tag{2.15}$$

and the dynamic condition (2.8) takes the form

$$D\frac{\partial\Phi_2}{\partial t} - \frac{\partial\Phi_1}{\partial t} + \tfrac{1}{2}D\left[\left(u^S + \frac{\partial\Phi_2}{\partial r}\right)^2 + \left(w^S + \frac{\partial\Phi_2}{\partial z}\right)^2\right]$$
$$-\tfrac{1}{2}\left[\left(u^S + \frac{\partial\Phi_1}{\partial r}\right)^2 + \left(w^S + \frac{\partial\Phi_1}{\partial z}\right)^2\right] + (D-1)\eta$$
$$= \tfrac{1}{2}(D-1)\frac{F^2}{\pi^2\beta^4} + (D-1)\left(1 - \frac{Ft}{\pi\beta^2}\right) \quad \text{on } z = \eta. \tag{2.16}$$

The functions $u^S$ and $w^S$ in these interfacial conditions (2.15) and (2.16) are the steady-state velocity components that have been defined in equations (2.12).

The solution of the equations for this mathematical model of the draining of a two-fluid system from a cylindrical tank therefore requires that the interfacial shape $z = \eta(r, t)$ be determined, along with the two perturbed potentials $\Phi_1$ and $\Phi_2$.

## 3    The Linearized Solution

For small Froude number $F$, it is possible to develop a linearized approximation to the equations of motion in section 2. The unknown functions are expressed as expansions in powers of $F$, in the forms

$$\begin{aligned}
\Phi_1(r, z, t) &= F\Phi_{11}(r, z, t) + \mathcal{O}(F^2) \\
\Phi_2(r, z, t) &= F\Phi_{21}(r, z, t) + \mathcal{O}(F^2) \\
\eta(r, t) &= 1 - (Ft)/(\pi\beta^2) + F\eta_1(r, t) + \mathcal{O}(F^2).
\end{aligned} \tag{3.1}$$

The coefficient $P_n^S$ in the steady-state solution (2.11) is recognized to be a quantity of order $F$ in magnitude, and expressed as $P_n^S = FP_{n1}^S$.

The first-order perturbation potentials $\Phi_{11}$ and $\Phi_{21}$ in equations (3.1) are found to satisfy Laplace's equations, as in equations (2.2) and (2.3), and

9

the modified bottom, side and top conditions (2.13), (2.5) and (2.14). The kinematic interfacial conditions (2.15) take the approximate linearized forms

$$\frac{\partial \eta_1}{\partial t} = W_1^S + \frac{\partial \Phi_{i1}}{\partial z}, \quad i = 1, 2 \quad \text{on } z = 1 \tag{3.2}$$

in which the axial component of the steady-state velocity in equation (2.12) has been expressed as

$$w^S(r, z) = -\frac{F}{\pi \beta^2} + FW_1^S(r, z). \tag{3.3}$$

The linearized dynamical condition (2.16) becomes

$$D\frac{\partial \Phi_{21}}{\partial t} - \frac{\partial \Phi_{11}}{\partial t} + (D - 1)\eta_1 = 0 \quad \text{on } z = 1. \tag{3.4}$$

As the two linearized perturbation velocity potentials satisfy Laplace's equations in their respective domains, they may be expressed in the forms

$$\begin{aligned}
\Phi_{11}(r, z, t) &= \sum_{n=1}^{\infty} P_{n1}(t) J_0\left(j_{1,n}\frac{r}{\beta}\right) \cosh\left(\frac{j_{1,n}}{\beta}z\right) \\
\Phi_{21}(r, z, t) &= \sum_{n=1}^{\infty} R_{n1}(t) J_0\left(j_{1,n}\frac{r}{\beta}\right) \cosh\left(\frac{j_{1,n}}{\beta}(1 + \lambda - z)\right).
\end{aligned} \tag{3.5}$$

The linearized interface elevation can similarly be written

$$\eta_1(r, t) = \sum_{n=1}^{\infty} H_{n1}(t) J_0\left(j_{1,n}\frac{r}{\beta}\right). \tag{3.6}$$

The use of the forms (3.5) and (3.6) in the two linearized kinematic conditions (3.2) give rise to the two sets of relationships

$$\begin{aligned}
H'_{n1}(t) &= \frac{j_{1,n}}{\beta}\left[P_{n1}(t)\sinh\left(\frac{j_{1,n}}{\beta}\right) - P_{n1}^S \sinh\left(\frac{j_{1,n}}{\beta}\lambda\right)\right] \\
R_{n1}(t) &= -P_{n1}(t)\frac{\sinh(j_{1,n}/\beta)}{\sinh(j_{1,n}\lambda/\beta)}, \quad n = 1, 2, 3, \ldots
\end{aligned} \tag{3.7}$$

between the Fourier coefficients in these expressions. The linearized dynamic condition (3.4) likewise gives the additional set of equations

$$\begin{aligned}
(D - 1)H_{n1}(t) &= P'_{n1}(t)\cosh(j_{1,n}/\beta) - DR'_{n1}(t)\cosh(j_{1,n}\lambda/\beta) \\
n &= 1, 2, 3, \ldots.
\end{aligned} \tag{3.8}$$

10

These three equations (3.7), (3.8) may be combined and solved for the three sets of Fourier coefficients in the expressions (3.5) and (3.6). In particular, the coefficients that determine the linearized interface shape may be shown to be determined from the differential equations

$$\frac{d^2 H_{n1}}{dt^2} + \Omega_{n1}^2 H_{n1} = 0, \quad n = 1, 2, 3, \ldots,$$

(3.9)

in which it is convenient to define the constants

$$\Omega_{n1}^2 = \frac{(1 - D)(j_{1,n}/\beta)}{D \coth(j_{1,n}\lambda/\beta) + \coth(j_{1,n}/\beta)}.$$

(3.10)

Clearly (3.9) are simple harmonic equations with sinusoidal solutions in time. For impulsive start of the sink at time $t = 0$, the appropriate initial conditions are

$$H_{n1}(0) = 0 \quad \text{and} \quad R_{n1}(0) = 0$$

so that, after some algebra, the linearized interface elevation may be obtained in the final form

$$\begin{aligned}
\eta(r, t) &= 1 - \frac{Ft}{\pi\beta^2} \\
&\quad - \frac{2F}{\pi\alpha\beta} \sum_{n=1}^{\infty} \frac{J_0(j_{1,n}r/\beta) J_1(j_{1,n}\alpha/\beta) \sinh(j_{1,n}\lambda/\beta) \sin(\Omega_{n1}t)}{\sinh(j_{1,n}(1+\lambda)/\beta) j_{1,n} \Omega_{n1} J_0^2(j_{1,n})} \\
&\quad + \mathcal{O}(F^2).
\end{aligned}$$

(3.11)

When the lower fluid is heavier than the upper one, so that $D < 1$, the constants $\Omega_{n1}$ in equation (3.10) are frequencies, and their physical meaning is related to the natural frequency at which a small packet of fluid would oscillate about the undisturbed interface level $y = 1$, if it were displaced from equilibrium. In that respect, the lowest frequency component $\Omega_{11}$ is the equivalent of a Brunt-Väisälä frequency (see Dutton [21] page 71 or Vallis [22] page 92).

# 4   The Non-Linear Solution Technique

The non-linear equations in section 2 cannot be solved in closed form, and so numerical methods are needed instead. In this section, we achieve this by adapting the highly accurate spectral method of Forbes *et al* [17] and Forbes and Hocking [16] to this purpose. The perturbation potentials $\Phi_1$ and $\Phi_2$ in

11

equation (2.9) are both solutions of Laplace's equation, and so are expressed in the approximate Fourier-series form

$$\Phi_1(r,z,t) = P_0(t) + \sum_{n=1}^{N} P_n(t) J_0\left(j_{1,n}\frac{r}{\beta}\right) \cosh\left(\frac{j_{1,n}}{\beta}z\right)$$

$$\Phi_2(r,z,t) = R_0(t) + \sum_{n=1}^{N} R_n(t) J_0\left(j_{1,n}\frac{r}{\beta}\right) \cosh\left(\frac{j_{1,n}}{\beta}(1+\lambda-z)\right). (4.1)$$

As the number of Fourier coefficients $N$ in these expressions increases, these approximations (4.1) become more accurate. The two zeroth-order coefficients $P_0$ and $R_0$ in these expressions are not both needed in the final solution, and in this work, we therefore set $R_0(t) = 0$ but solve for $P_0(t)$ along with the other coefficients.

It is convenient at this point to define perturbation velocity components in the radial and axial directions in both fluids. These are written as

$$U_1 = \frac{\partial \Phi_1}{\partial r} = -\sum_{n=1}^{N} \frac{j_{1,n}}{\beta} P_n(t) J_1\left(j_{1,n}\frac{r}{\beta}\right) \cosh\left(\frac{j_{1,n}}{\beta}z\right)$$

$$W_1 = \frac{\partial \Phi_1}{\partial z} = \sum_{n=1}^{N} \frac{j_{1,n}}{\beta} P_n(t) J_0\left(j_{1,n}\frac{r}{\beta}\right) \sinh\left(\frac{j_{1,n}}{\beta}z\right)$$

$$U_2 = \frac{\partial \Phi_2}{\partial r} = -\sum_{n=1}^{N} \frac{j_{1,n}}{\beta} R_n(t) J_1\left(j_{1,n}\frac{r}{\beta}\right) \cosh\left(\frac{j_{1,n}}{\beta}(1+\lambda-z)\right)$$

$$W_2 = \frac{\partial \Phi_2}{\partial z} = -\sum_{n=1}^{N} \frac{j_{1,n}}{\beta} R_n(t) J_0\left(j_{1,n}\frac{r}{\beta}\right) \sinh\left(\frac{j_{1,n}}{\beta}(1+\lambda-z)\right). (4.2)$$

These functions (4.2), along with their steady-state equivalents (2.12) will be evaluated along the interface and used extensively in the following development.

As the geometry of this problem is axially symmetric, it is possible to represent the interface parametrically in terms of an arclength $s$, defined in the usual Pythagorean manner

$$ds^2 = dr^2 + dz^2. \tag{4.3}$$

At the tank centre $r = 0$, we impose the condition $s = 0$ and at the tank walls $r = \beta$ the interface length has some unknown value $s = L(t)$. Rather than using $s$ in equation (4.3) directly, however, it is instead more convenient to define a scaled arclength

$$\xi = \beta s/L(t). \tag{4.4}$$

12

This quantity $\xi$ in equation (4.4) was introduced by Forbes *et al* [17] and has the advantage that it takes the known values $\xi = 0$ at $r = 0$ and $\xi = \beta$ at $r = \beta$. The use of this variable in a parametric representation of the interface permits us to compute solutions in which the interface could fold over and become multi-valued, although no such behaviour has in fact been encountered here.

In terms of the scaled arclength (4.4), the interface shape may now be represented in the parametric form

$$
\begin{aligned}
r(\xi, t) &= \xi + \sum_{n=1}^{N} A_n(t) J_1\left(j_{1,n}\frac{\xi}{\beta}\right) \\
\eta(\xi, t) &= 1 - \frac{Ft}{\pi\beta^2} + C_0(t) + \sum_{n=1}^{N} C_n(t) J_0\left(j_{1,n}\frac{\xi}{\beta}\right).
\end{aligned}
\tag{4.5}
$$

This introduces two additional sets of coefficients $A_n$ and $C_n$ that must be found, along with $P_n$ and $R_n$ in equations (4.1), in the numerical solution process.

The arclength condition (4.3) leads to the additional equation

$$
\left(\frac{\partial r}{\partial \xi}\right)^2 + \left(\frac{\partial \eta}{\partial \xi}\right)^2 = \frac{L^2(t)}{\beta^2}
\tag{4.6}
$$

along the interface. This equation is now subjected to Fourier-Bessel decomposition, to derive a system of equations involving the unknown time-dependent coefficients.

The zeroth-order terms are obtained simply by multiplying throughout by the variable $\xi$ and integrating over the domain $0 < \xi < \beta$. This leads at once to

$$
L(t) = \sqrt{2 \int_0^\beta \xi \left[\left(\frac{\partial r}{\partial \xi}\right)^2 + \left(\frac{\partial \eta}{\partial \xi}\right)^2\right] d\xi},
\tag{4.7}
$$

which is an expression for determining the unknown surface length $L(t)$.

Differential equations for the higher order modes are obtained by differentiating the arclength condition (4.6) with respect to time, giving

$$
\left(\frac{\partial r}{\partial \xi}\right)\left(\frac{\partial^2 r}{\partial \xi \partial t}\right) + \left(\frac{\partial \eta}{\partial \xi}\right)\left(\frac{\partial^2 \eta}{\partial \xi \partial t}\right) = \frac{L(t)L'(t)}{\beta^2}.
\tag{4.8}
$$

This equation (4.8) is now multiplied in turn by the functions $\xi J_0(j_{1,k}\xi/\beta)$, $k = 1, 2, \ldots, N$ and integrated. After making use of recurrence relations for

13

Bessel functions, as found in Abramowitz and Stegun [20], there results the system of differential equations

$$\sum_{n=1}^{N} \frac{j_{1,n}}{\beta} \mathcal{M}_{kn} A'_n(t) - \sum_{n=1}^{N} \frac{j_{1,n}}{\beta} \mathcal{N}_{kn} C'_n(t) = 0 \quad k = 1, \ldots, N \qquad (4.9)$$

involving time derivatives of the two sets of coefficients $A_n(t)$ and $C_n(t)$. The Fourier decomposition process leads to intermediate quantities $\mathcal{M}_{kn}$ and $\mathcal{N}_{kn}$ involving integrals of quantites evaluated along the interface, and these are given in the Appendix.

The two kinematic conditions (2.15) are next subject to similar Fourier-Bessel decomposition. Firstly, however, they need to be expressed in parametric form along the interface, making use of the variable $\xi$ in equation (4.4). It follows from the chain rule of calculus that

$$\left(\partial\eta/\partial r\right)_t = \frac{\left(\partial\eta/\partial\xi\right)_t}{\left(\partial r/\partial\xi\right)_t}, \qquad (4.10)$$

in which the subscripts show the variables that are to be held constant during the indicated differentiations. Similarly,

$$\left(\partial\eta/\partial t\right)_r = \left(\partial\eta/\partial t\right)_\xi - \frac{\left(\partial\eta/\partial\xi\right)_t \left(\partial r/\partial t\right)_\xi}{\left(\partial r/\partial\xi\right)_t}. \qquad (4.11)$$

The first kinematic condition in the system (2.15) becomes

$$\left(w^S + W_1\right)\left(\frac{\partial r}{\partial\xi}\right)_t = \left(\frac{\partial\eta}{\partial t}\right)_\xi \left(\frac{\partial r}{\partial\xi}\right)_t - \left(\frac{\partial\eta}{\partial\xi}\right)_t \left(\frac{\partial r}{\partial t}\right)_\xi + \left(u^S + U_1\right)\left(\frac{\partial\eta}{\partial\xi}\right)_t \qquad (4.12)$$

after making use of equations (4.10) and (4.11). The second equation in the system (2.15) is replaced by the difference of the two kinematic conditions, and can be expressed as

$$\left(W_2 - W_1\right)\left(\partial r/\partial\xi\right)_t = \left(U_2 - U_1\right)\left(\partial\eta/\partial\xi\right)_t. \qquad (4.13)$$

The chain rule relations (4.10) and (4.11) have again been used in the derivation of (4.13), and the velocity components are as defined in the relations (2.12) and (4.2).

To obtain the zeroth-order term in the Fourier-Bessel decomposition of the first kinematic condition (4.12), the equation is multiplied by $r$ and integrated over the domain $0 < \xi < \beta$. Integration by parts yields the elegant result

$$\int_0^\beta r\left(\frac{\partial r}{\partial\xi}\right)\left(w^S + W_1\right) d\xi = \int_0^\beta r\left(\frac{\partial\eta}{\partial\xi}\right)\left(u^S + U_1\right) d\xi - \frac{F}{2\pi} \qquad (4.14)$$

14

after use has been made of the appropriate recurrence relations for Bessel functions, and the series representations (2.12) and (4.2) for the velocity components evaluated on the interface. The zeroth-order term from equation (4.12) now yields

$$C_0'(t) = \frac{2}{\beta^2}\left[\sum_{n=1}^{N}\mathcal{H}_{0n}A_n'(t) - \sum_{n=1}^{N}\mathcal{R}_{0n}C_n'(t)\right], \qquad (4.15)$$

and again involves derivatives of the sets of coefficients $A_n(t)$ and $C_n(t)$. The intermediate quantities $\mathcal{H}_{0n}$ and $\mathcal{R}_{0n}$ are available from the Appendix.

The higher order modes in the decomposition of the first kinematic condition (4.12) may be obtained in a similar manner, by multiplying by $rJ_0\big(j_{1,k}\xi/\beta\big)$, $k = 1, \ldots, N$ and integrating. Integration by parts is again used, as in equation (4.14), and after some algebra, the system of differential equations

$$\sum_{n=1}^{N} T_{kn}^{(1)} A_n'(t) - \sum_{n=1}^{N} T_{kn}^{(2)} C_n'(t)$$
$$= (j_{1,k}/\beta)\sum_{n=1}^{N}\big(S_{kn}^{(2)}P_n^S - S_{kn}^{(1)}P_n(t)\big) \quad k = 1, \ldots, N \qquad (4.16)$$

is obtained. It involves additional sets of intermediate functions, which are given for completeness in the Appendix.

The second kinematic condition, written in the form (4.13), is subjected to the same process of Fourier-Bessel decomposition. Integration by parts yields the elegant identity

$$\int_0^\beta r\big(W_2 - W_1\big)\left(\frac{\partial r}{\partial \xi}\right) d\xi = \int_0^\beta r\big(U_2 - U_1\big)\left(\frac{\partial \eta}{\partial \xi}\right) d\xi,$$

so that the zeroth-order mode is satisfied identically.

The higher-order modes are derived, as before, by multiplying equation (4.13) by $rJ_0\big(j_{1,k}\xi/\beta\big)$, $k = 1, \ldots, N$ and integrating. After making use of integration by parts and recurrence relations for Bessel functions, the remarkably simple result

$$\sum_{n=1}^{N}\left[S_{kn}^{(1)}P_n(t) + S_{kn}^{(2)}R_n(t)\right] = 0, \quad k = 1, \ldots, N \qquad (4.17)$$

is obtained as an identity. The functions $S_{kn}^{(1)}$ and $S_{kn}^{(2)}$ are as defined in equation (8.3) in the Appendix.

15

In spite of its elegance, however, the identity (4.17) is not in a convenient form for use in a numerical solution technique. To avoid having to solve a differential–algebraic system of equations, the result (4.17) is differentiated with respect to time $t$. After a significant amount of algebra, this results in a system of differential equations of the form

$$\sum_{n=1}^{N}\left[-K_{kn}A_n'(t) + L_{kn}C_n'(t) + S_{kn}^{(1)}P_n'(t) + S_{kn}^{(2)}R_n'(t)\right]$$
$$= \frac{F}{\pi\beta^2}\int_0^\beta rJ_1\left(j_{1,k}\frac{\xi}{\beta}\right)(U_2 - U_1)\,d\xi \quad k = 1, \ldots, N. \tag{4.18}$$

Use has again been made of the functions (8.3) in the Appendix. In addition, there are two further sets of quantities $K_{kn}(t)$ and $L_{kn}(t)$ in this result (4.18), which are presented in the Appendix. Appropriate use has again been made of the relevant recurrence relations for Bessel functions, along with equation (4.15) to eliminate the quantity $C_0'(t)$.

Finally, the dynamic interfacial condition (2.16) is subjected to the similar decomposition. The condition may be expressed in the form

$$D\sum_{n=1}^{N}R_n'(t)J_0\left(j_{1,n}\frac{r}{\beta}\right)\cosh\left(j_{1,n}\frac{(1+\lambda-\eta)}{\beta}\right)$$
$$- P_0'(t) - \sum_{n=1}^{N}P_n'(t)J_0\left(j_{1,n}\frac{r}{\beta}\right)\cosh\left(j_{1,n}\frac{\eta}{\beta}\right)$$
$$+ \tfrac{1}{2}D\left[\left(u^S + U_2\right)^2 + \left(w^S + W_2\right)^2\right] - \tfrac{1}{2}\left[\left(u^S + U_1\right)^2 + \left(w^S + W_1\right)^2\right]$$
$$= (D-1)\left[\frac{F^2}{2\pi^2\beta^4} - C_0(t) - \sum_{n=1}^{N}C_n(t)J_0\left(j_{1,n}\frac{\xi}{\beta}\right)\right]. \tag{4.19}$$

As before, the zeroth order Fourier decomposition of the dynamic condition is obtained by multiplying equation (4.19) by $\xi$ and integrating. This gives the ordinary differential equation

$$-\tfrac{1}{2}\beta^2 P_0'(t) - \sum_{n=1}^{N}G_{0n}^{(1)}P_n'(t) + D\sum_{n=1}^{N}G_{0n}^{(2)}R_n'(t)$$
$$= \tfrac{1}{2}J_0^{(1)} - \tfrac{1}{2}DJ_0^{(2)} + (D-1)\left[\frac{F^2}{4\pi^2\beta^2} - \tfrac{1}{2}\beta^2 C_0(t)\right]. \tag{4.20}$$

16

Similarly, the higher order decomposition gives rise to the system of equations

$$
\begin{aligned}
&-\sum_{n=1}^{N} G_{kn}^{(1)} P_n'(t) + D \sum_{n=1}^{N} G_{kn}^{(2)} R_n'(t) \\
&= \tfrac{1}{2} J_k^{(1)} - \tfrac{1}{2} D J_k^{(2)} - \tfrac{1}{2}(D-1)\beta^2 J_0^2(j_{1,k}) C_k(t) \\
&\quad k = 1, \ldots, N.
\end{aligned}
\tag{4.21}
$$

The relevant intermediate quantities in these expressions are presented in the Appendix.

Equations (4.9), (4.15), (4.16), (4.18), (4.20) and (4.21) constitute a system of $4N + 2$ simultaneous ordinary differential equations for the Fourier coefficients $A_n$, $C_0$, $C_n$, $P_n$, $P_0$ and $R_n$, $n = 1, 2, \ldots, N$. The system is solved here using the straightforward fourth-order Runge-Kutta scheme, outlined in the text by Atkinson [23] page 371. At each step in the process, a matrix equation must be solved, and this is what takes most of the computer run-time for the algorithm. In addition, the intermediate functions in equations (4.7) along with (8.1), (8.2), (8.3), (8.4) and (8.5) in the Appendix require the evaluation of integrals, and this is done here using Gauss-Legendre quadrature. The numerical abscissae and weights have been computed using the algorithm written by Greg von Winckel, and made available on the MATLAB file exchange site [24] (although the method was converted to FORTRAN for use in our code). It has been found here that 201 quadrature points is sufficient to give very good accuracy in the evaluation of the integrals, and $N = 51$ Fourier-Bessel coefficients are used for accuracy in these results.

# 5   Results for Sink Flow

## 5.1   Stable withdrawal

We begin this section with an investigation of the situation in which fluid is withdrawn from lower fluid 1, so that $F > 0$. The two-fluid system is stable, with upper fluid 2 being lighter than that in the lower layer, and this is expressed by the inequality $D < 1$.

Figure 2 shows a comparison of the linearized and non-linear interface height at the centre of the tank, on the axis $r = 0$, for the stable density ratio $D = 0.99$. In this example, the radius of the drain hole is $\alpha = 0.5$, the tank has radius $\beta = 20$ and the Froude number is $F = 0.1$. The initial depth of upper layer 2 has been chosen to be $\lambda = 2/3$. The linearized result has been obtained by numerical computation of the series expression (3.11)
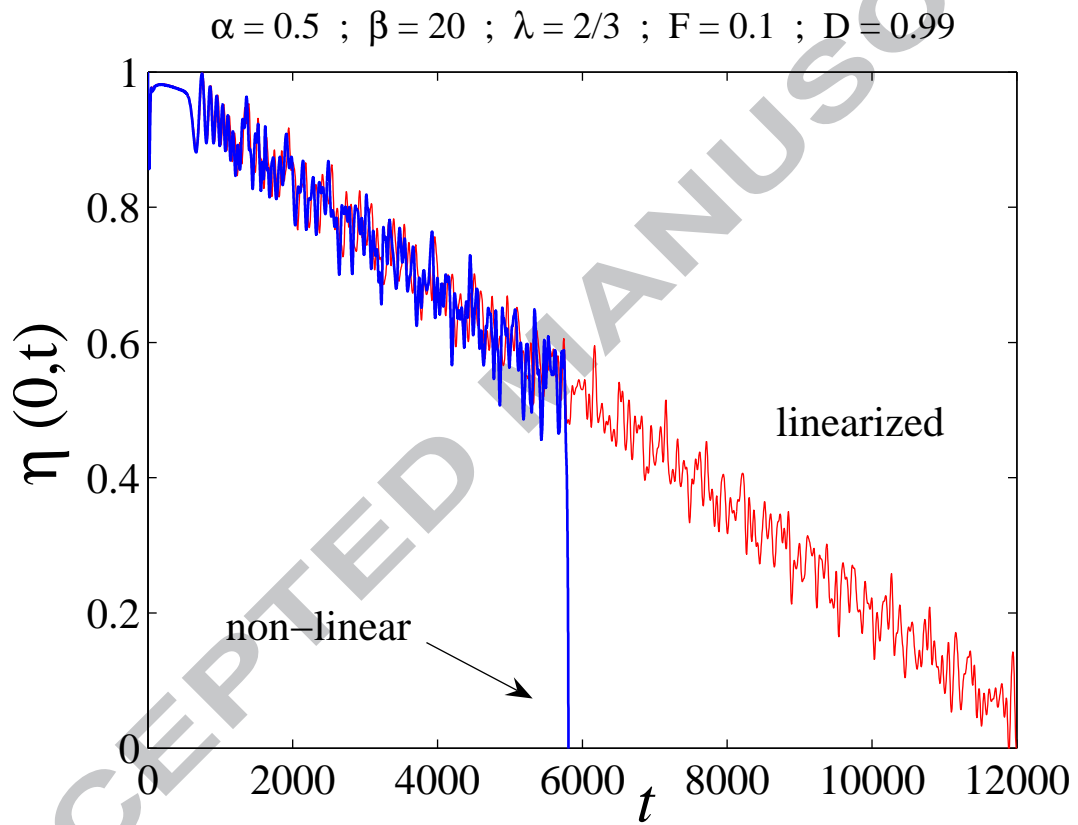
17

Figure 2: A comparison of the centre-line interface height computed by the linearized and non-linear solutions, for density ratio $D = 0.99$, hole radius $\alpha = 0.5$ and Froude number $F = 0.1$.

evaluated with $r = 0$, and the non-linear solution has been computed using the spectral algorithm described in section 4.

Both the linearized and non-linear interface heights at $r = 0$ show a large number of small-amplitude oscillations, representing the effects of the initial impulsive withdrawal of fluid at $t = 0$ and the subsequent generation of a sequence of high frequency waves that are reflected from the tank walls at $r = \beta$ and re-focussed at the centre $r = 0$. For earlier times, there is excellent agreement between the two solutions, and this gives confidence in the reliability of the non-linear algorithm in section 4. In fact, the two sets of results are almost indistinguishable up until about $t = 2,000$; after that time they begin to differ, although only slightly. However, the non-linear solution then suddenly collapses into the drain hole at about the time $t = 5,807$, but there is no equivalent to this phenomenon in the corresponding linearized approximation, which simply predicts that the interface should continue its essentially uniform progress toward the bottom of the tank.

Some details of the process outlined in Figure 2 are illustrated for the non-linear solution in Figure 3. The radial coordinate $r$ from the centre of the tank is plotted on the horizontal axis, and the height $z$ above the tank bottom appears on the vertical axis. Interface profiles are shown at seven different times, leading up to the moment at which the interface itself is withdrawn into the sink and the mathematical model in section 2 ceases to have any further validity.

Initially, the interface is horizontal and lies along the plane $z = 1$. The impulsive starting of the sink causes a narrow disturbance to the interface near $r = 0$, and as time progresses, this moves outward from the centre. This feature is evident in the first profile at $t = 63$ shown in Figure 3. For later times, the interface level drops more or less uniformly, as might be expected from the linearized solution (3.11), although it is evident from Figure 3 that the level at the centre $r = 0$ flicks up and down rapidly about the mean height, due to the arrival of reflected waves from the tank walls that are focussed at the tank centre-line, consistently with the results illustrated in Figure 2. The profile shown at time $t = 5,752$ is unremarkable except for the presence of a small upward jet at the centre $r = 0$, and this feature is consistent with earlier work of Zhou and Graebel [13] and Stokes *et al* [12]. However, at the slightly later time $t = 5,807$, non-linear effects have resulted in the sudden formation of a downwardly moving jet, and the consequent collapse of the interface into the drain hole. This is consistent with the overall behaviour reported by Zhou and Graebel [13] for narrow drain holes.

Figure 4 shows a comparison of the predictions of the linearized theory in equation (3.11) with the fully non-linear results from section 4, for a significantly wider drain hole of radius $\alpha = 2$. The linearized theory again predicts
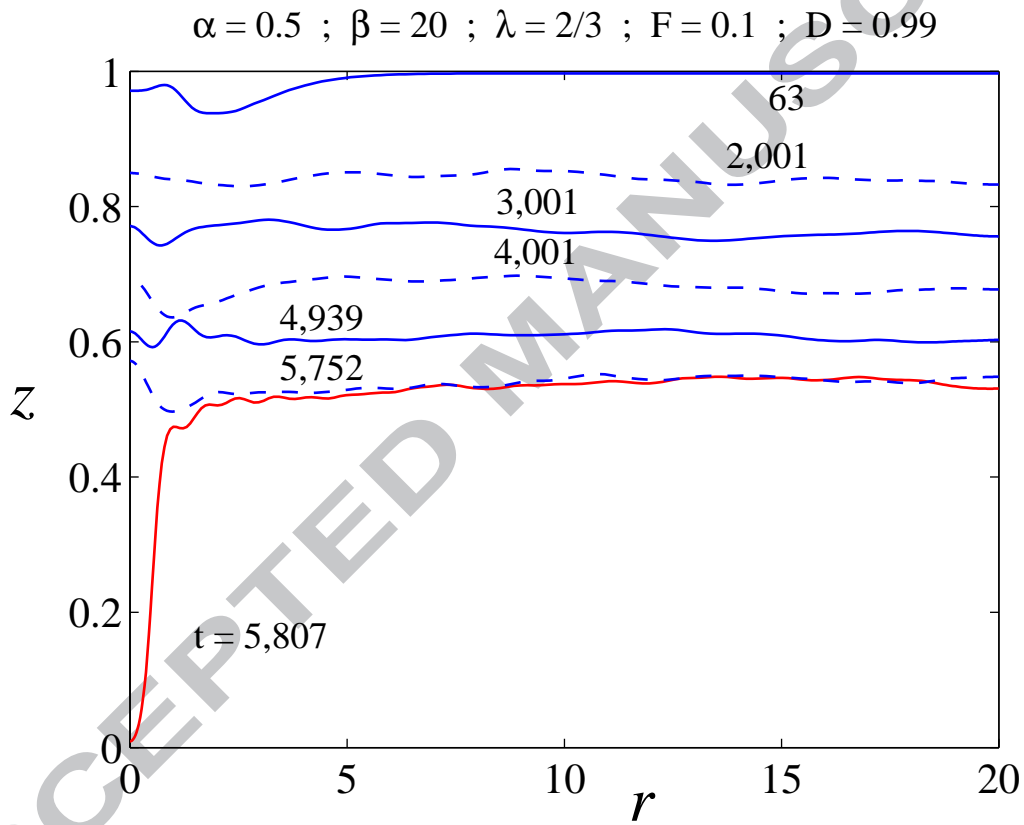
Figure 3: Interface elevations for the non-linear solution illustrated in Figure 2, at seven different times during the flow.
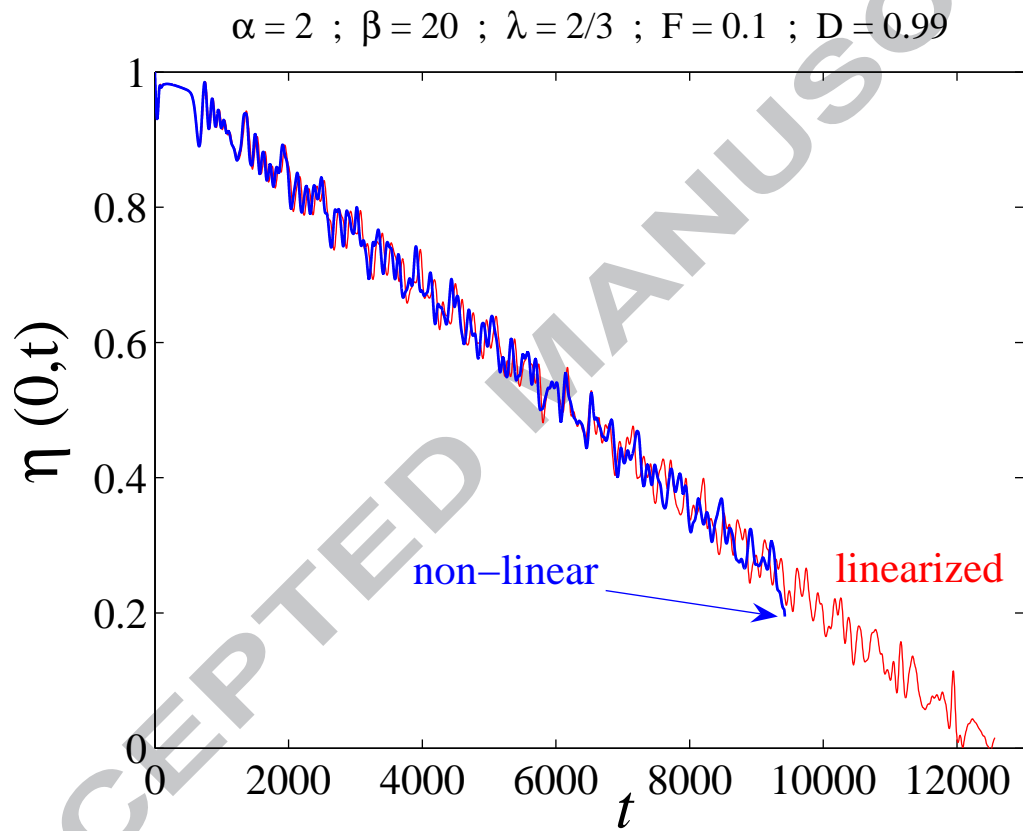
Figure 4: A comparison of the centre-line interface height computed by the linearized and non-linear solutions, for density ratio $D = 0.99$, hole radius $\alpha = 2$ and Froude number $F = 0.1$.
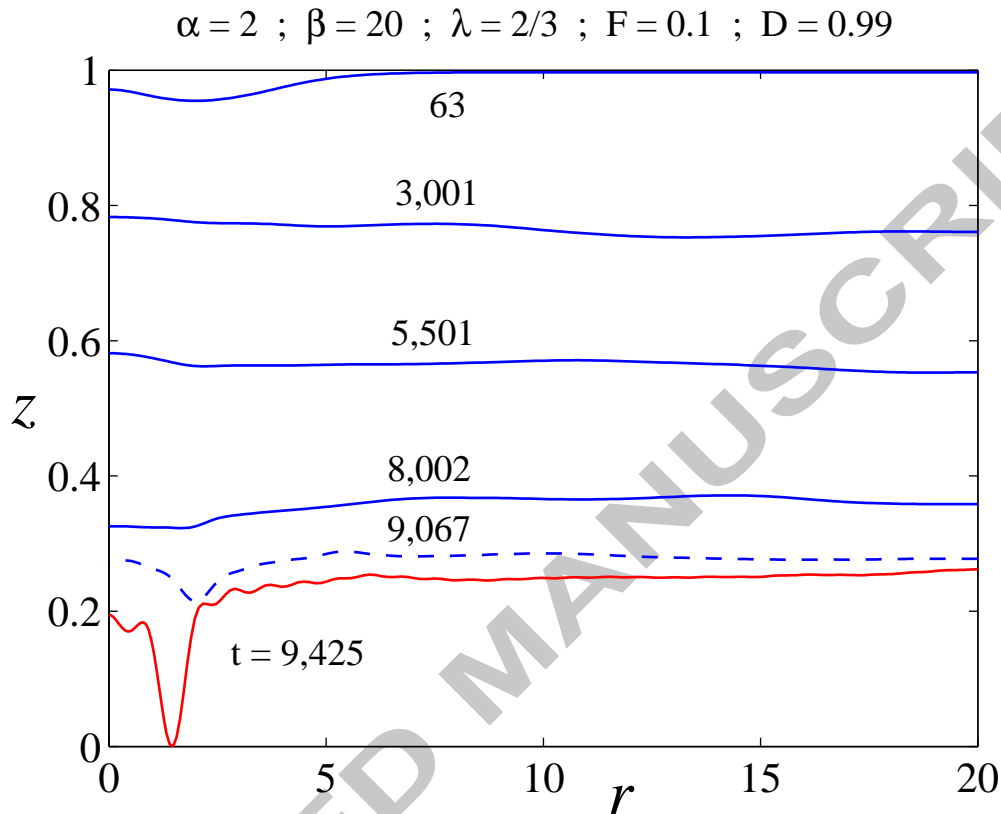
21

Figure 5: Interface elevations for the non-linear solution illustrated in Figure 4, at six different times during the flow.

that the mean interface height drops uniformly with time, although at the centre $r = 0$ there are high-frequency oscillations caused by reflection of disturbances from the tank walls at $r = \beta$. A similar effect was encountered in Figure 2. For the wider drain in Figure 4, there is again very good agreement indeed between the linearized and non-linear results up until at least time $t = 2,000$, and in fact the agreement is quite good even until $t = 6,000$. After that time, the non-linear results for the centre-line interface elevation begin to deviate somewhat from the linearized prediction, although the dramatic difference between them seen in Figure 2 is never encountered here in Figure 4. The non-linear solution fails abruptly at about time $t = 9,425$.

To understand the sudden failure of the non-linear solution at the time $t = 9,425$, it is instructive to study the full interface profiles. Some of these are presented in Figure 5, for the wider drain radius $\alpha = 2$ discussed in Figure 4. For the six profiles shown, the interface is seen to drop as time progresses,

as predicted by the linearized solution (3.11), and small-amplitude waves may also be visible. The elevation at the centre $r = 0$ moves up and down with time, as is evident from Figure 4, but no other features of note occur until the profile at time $t = 9,067$, when a downward-facing dimple appears at about the radius $r = 2$. For slightly later times, this then grows rapidly, and the interface pulls down into the sink, at the edge $r = \alpha$ of the circular drain hole in the bottom of the tank. The interface reaches the bottom at about time $t = 9,425$, and the model in section 2 fails to have validity for later times.

It follows from the results in Figure 5 that, in the last stages of the flow before the interface is drawn into the drain hole, there is an effective upwardly-facing region of lower fluid 1 near the tank centre $r = 0$, surrounded by the downwardly-moving ring at about radius $r = \alpha$. This is consistent with the results of Zhou and Graebel [13] for axi-symmetric flows, and was also encountered in two-dimensional (planar) withdrawal flows by Stokes *et al* [5] and Forbes and Hocking [16] under appropriate circumstances. It is possible to compute the curvature of the interfacial surface, using results from the article by Wehausen and Laitone [25], and we have in fact done this here. Details will not be presented in the interests of brevity, but it is found that the curvature does become large at the region near $r = \alpha$ where the interface is drawn into the sink. Zhou and Graebel [13] and Forbes and Hocking [16] suggested this may be evidence of the possible formation of a curvature singularity in the interface profiles under appropriate circumstances; when viscosity is re-introduced into the model, it is possible that the interface may then even overturn and roll up near these regions, similar to behaviour encountered in the famous Kelvin-Helmholtz instability by Moore [26] and Krasny [27], and for the Rayleigh-Taylor instability by Tryggvason [28], for example.

Results have also been generated for wider drain holes (larger values of $\alpha$). These show no new phenomena, however, and so are not reported here. As in Figure 5, it is found that the interface eventually draws down to the bottom of the tank at about the edge $r = \alpha$ of the drain hole, and that the phenomenon occurs over a short time interval at the termination of the flow. Agreement with the linearized theory is very good over a long time interval, however, and it is only really in these final stages of the flow that non-linear effects become important as the interface draws abruptly into the drain.

## 5.2 Unstable withdrawal

When the density ratio $D > 1$, the upper fluid in layer 2 is heavier than the lower fluid in layer 1, and it is then to be expected that the interface will be

unstable even to small-amplitude perturbation. This is closely related to the famous Rayleigh-Taylor instability discussed in the text by Chandrasekhar [29], and more recently by Forbes [30], [31]. In the present case, flow with $D > 1$ corresponds to a Rayleigh-Taylor type situation in which a background flow is also present. When $D > 1$, the linearized solution (3.11) is still valid, at least for initial times. The quantities $\Omega_{n1}^2$ in equation (3.10) become negative, but the ratios $\sin(\Omega_{n1}t)/\Omega_{n1}$ in equation (3.11) remain real, so that the linearized result for $\eta(r, t)$ retains validity. However, the interfacial elevation $\eta$ in equation (3.11) grows exponentially with time for $D > 1$, and the mathematical expression may become either large and positive or large and negative as time increases, depending on the ratio $\alpha/\beta$. Thus the linearized solution for the interface elevation at a fixed value of $r$ may either grow until it meets the top of the tank or else be drawn down to the tank bottom depending on the value of $\alpha/\beta$, in the case $D > 1$.

Figure 6 shows the results of three non-linear solutions obtained for the three values $\alpha = 0.5$, 2 and 4 of the drain radius. For these solutions, the density ratio has the value $D = 1.01$, so that these are all flows of essentially Rayleigh-Taylor type. The linearized solution computed from equation (3.11) is also shown for each case as indicated, and is drawn with thinner lines. For the narrow drain hole $\alpha = 0.5$, the interface at the centre of the tank is withdrawn uniformly downwards into the hole, and the entire process is completed by about time $t = 30$. This may be contrasted with the same situation shown in Figure 2 although for the stable case $D = 0.99$, where withdrawal of the interface at the centre took about $t = 5,807$ dimensionless time units. For the unstable case with $D = 1.01$ shown in Figure 6, a downward-directed jet is formed near the centre $r = 0$ of the tank, and this is withdrawn very rapidly into the drain, in the case $\alpha = 0.5$ when the drain is narrow.

The situation for unstable withdrawal and wider drain holes shown in Figure 6 is somewhat more interesting. The interface height at the centre $r = 0$ of the tank is not necessarily withdrawn to the bottom of the tank, and may even form an upward-directed jet while the fluid in lower layer 1 is being removed overall. This is possible because unstable waves may be produced over the disk $r < \alpha$ above the drain hole, and their amplitude grows with time. Thus the two curves for $\alpha = 2$ and $\alpha = 4$ in Figure 6 initially indicate a slight drop in the level $\eta(0, t)$ of the interface at the tank centre, but then show the development of large-amplitude unstable oscillations at later times, before the solution fails. It is clear that, for all three solutions in Figure 6, the linearized solution (3.11) gives an accurate description of this unstable flow for early times, but may eventually become more inaccurate as time increases. This is as expected, since for $D > 1$ disturbances grow with time,
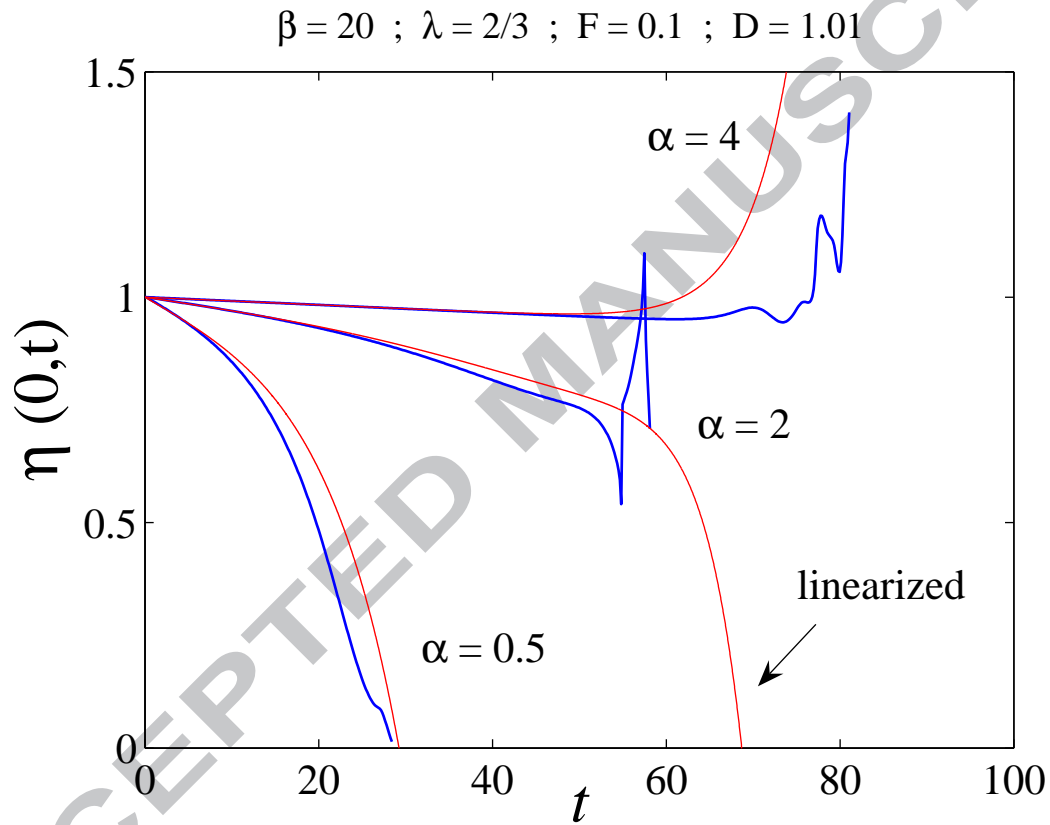
24

Figure 6: Centre-line interfacial heights computed for three non-linear solutions, for density ratio $D = 1.01$, and drain radii $\alpha = 0.5$, 2 and 4. Results are obtained with Froude number $F = 0.1$. The linearized solutions are also shown for the same three cases.

25

$\alpha = 2 \; ; \; \beta = 20 \; ; \; \lambda = 2/3 \; ; \; F = 0.1 \; ; \; D = 1.01$
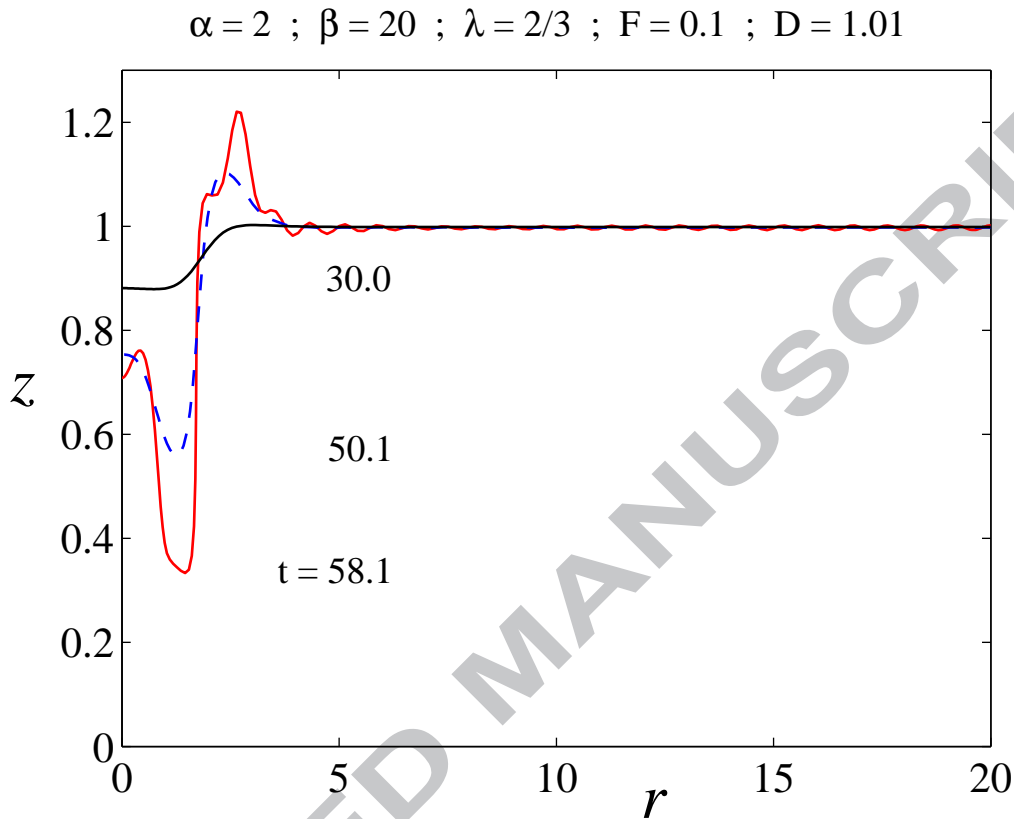


Figure 7: Interface elevations for the non-linear solution with drain width $\alpha = 2$ illustrated in Figure 6, at three different times during the flow.

so that the small perturbation assumption of linearized theory ceases to be valid as time progresses.

Details of the non-linear behaviour summarized in Figure 6, for wider drains, are shown in Figures 7 and 8. For the case with $\alpha = 2$ illustrated in Figure 7, the interface at the tank centre is initially drawn down, but at a later time forms an upwardly-directed jet before moving down again. The interface profile for $t = 58.1$ represents the largest time for which the numerical scheme in section 4 could yield a solution, and is clearly close to a time at which the model itself fails. This appears to be due to the formation of an upwardly-directed region of very high curvature at about $r = 3$, at approximate height $z = 1.2$. It seems likely that a curvature singularity is about to form at this point, and so the re-introduction of viscosity into the model may then lead to interface overhang or roll-up at slightly later times.

Figure 8 shows the development of some interface profiles for the widest
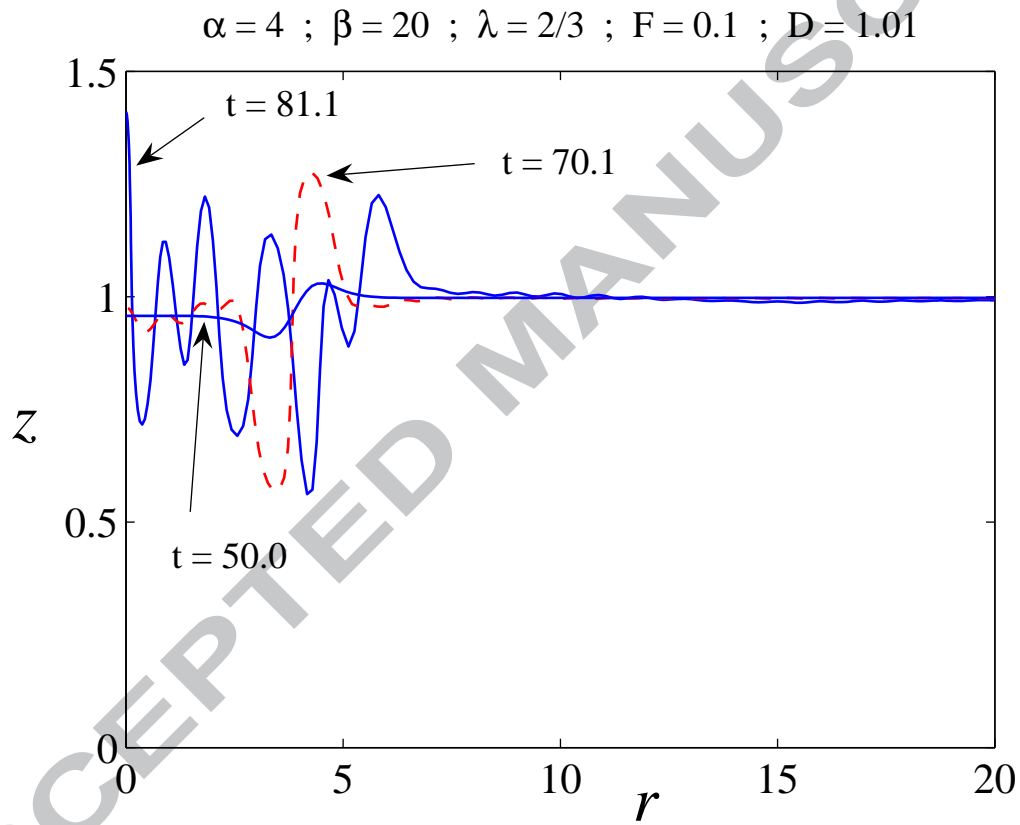
26

Figure 8: Interface elevations for the non-linear solution with drain width $\alpha = 4$ illustrated in Figure 6, at three different times during the flow.

27

drain $\alpha = 4$ depicted in Figure 6. A dip in the interface initially appears at about the edge of the drain hole, at $r = 4$, and this rapidly grows in amplitude. The last time for which the numerical method of section 4 could yield a solution was $t = 81.1$, and it is evident that a packet of non-linear waves has developed above the drain hole region. A very sharp upwardly-directed jet has formed at the centre of the tank, at $r = 0$, and it would appear that the failure of the solution for later times is due either to the formation of a curvature singularity at this point, or else to the possibility that the interface itself might move to the top of the tank at $z = 1 + \lambda$. In any event the situation is highly unstable, even for this density ratio $D = 1.01$ that is so close to unity, and so slight changes to the initial conditions of impulsive start of the sink would no doubt give very different outcomes in Figures 6–8.

# 6  Results for Source Flow

## 6.1  Stable injection

It is possible also to consider the model in section 2 as representing the case in which fluid is injected into lower layer 1 through the hole in the tank bottom, rather than being withdrawn through it. This may be achieved simply by allowing the Froude number $F$ in (2.1) to be negative. The linearized solution in equation (3.11) similarly retains validity for $F < 0$.

In Figure 9, the time histories of two different solutions are shown. In each case, the Froude number is $F = -0.1$ and the hole radius is $\alpha = 0.5$, corresponding to fluid injection through a narrow pipe in the bottom of the tank. For the solution on the right of the figure, the density ratio is $D = 0.99$, so that this represents a stable two-fluid system with the lighter fluid on the top. It persists until about $t = 8,252$, after which time some portion of the interface meets the top of the tank at $z = 1 + \lambda$ and the solution then ceases to be valid. The linearized solution (3.11) agrees closely with this non-linear result until about time $t = 2,000$, and the two solutions then remain reasonably similar over the entire time interval shown. The linearized solution is not shown here, however, as it is difficult to distinguish from the non-linear case, and obscures the view of both. The solution to the left of the diagram has been computed with $D = 1.01$, and so corresponds to the unstable Rayleigh-Taylor type situation in which upper fluid 2 is the heavier. It ceases to be valid after the much shorter time $t = 37.7$, when again some portion of the interface reaches the top of the tank.

Some interface profiles corresponding to the stable injection flow with

28

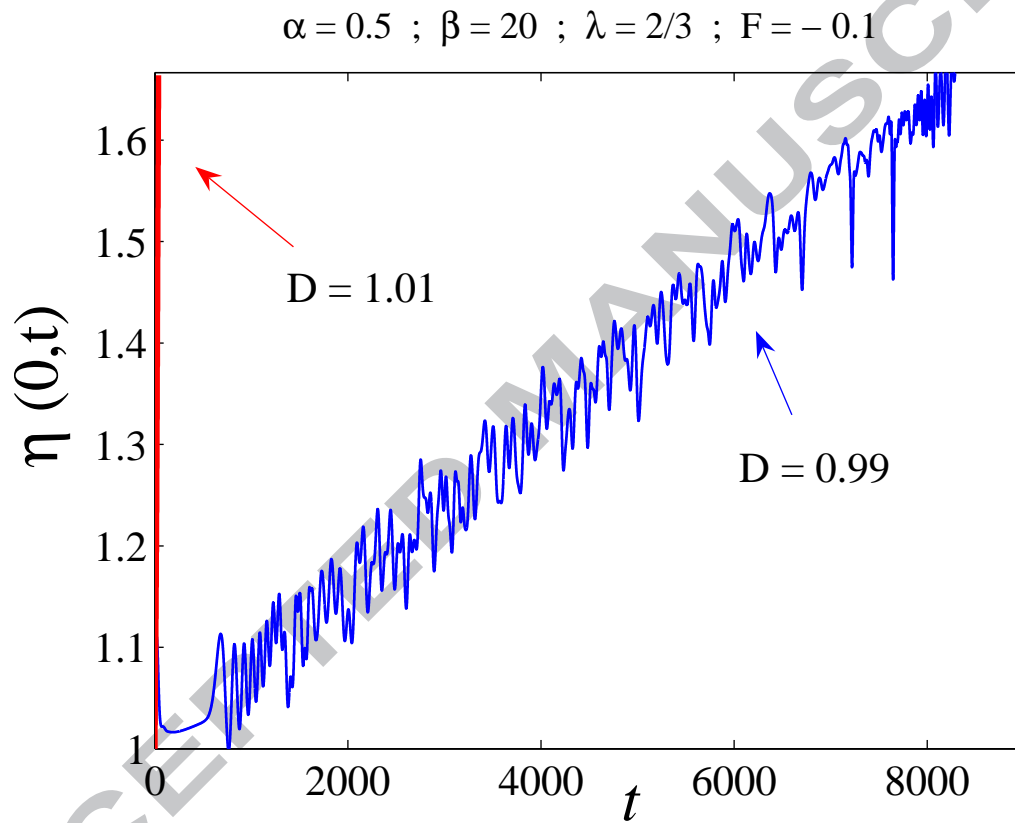$$\alpha = 0.5 \; ; \; \beta = 20 \; ; \; \lambda = 2/3 \; ; \; F = -0.1$$



Figure 9: Non-linear centre-line interfacial heights computed for drain radius $\alpha = 0.5$, and for the two values of density ratio $D = 0.99$ (stable injection) and $D = 1.01$ (unstable injection). Both results are obtained with Froude number $F = -0.1$.
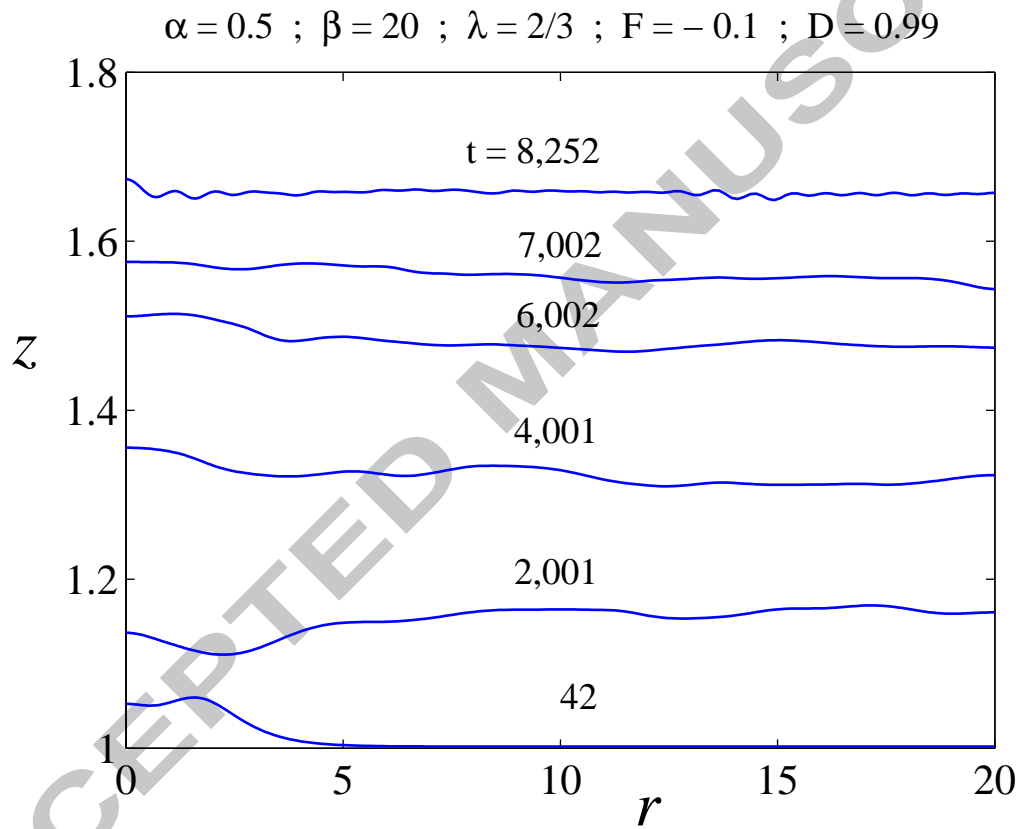
Figure 10: Six interface elevations for the stable non-linear solution with density ratio $D = 0.99$ illustrated in Figure 9. The injection hole radius is $\alpha = 0.5$.

30

$D = 0.99$ in Figure 9 are shown in Figure 10. At the first time $t = 42$ shown, the effect of the impulsive start of the sink can be seen as an elevation near the centre $r = 0$ of the tank. As time progresses, the mean level of the interface rises uniformly, as expected by conservation of mass, although small waves may be seen on the profiles. The elevation at the centre exhibits more rapid oscillations, due to the reflection of the waves from the tank walls and the focussing of those waves at the tank centre, as a consequence of the cylindrically symmetric geometry in this flow. Eventually, the interface meets the top of the tank at about time $t = 8,252$, and thereafter the model in section 2 ceases to be valid.

## 6.2   Unstable injection

The final circumstance to be considered in this paper is that corresponding to injection of fluid through the hole on the tank bottom, in the unstable case $D > 1$. This is essentially a Rayleigh-Taylor flow with heavier fluid being pushed upward by a lighter fluid from below. A sample calculation has been presented in Figure 9, for the interface elevation at the centre of the tank.

Figure 11 shows interface profiles at four different times, for the case $D = 1.01$ illustrated in Figure 9. For this unstable flow, a vertical jet forms near the tank centre $r = 0$ in response to the impulsive start of the source, and its amplitude then grows rapidly with time until about $t = 37.7$ when it intersects the top of the tank.

For a wider injection hole, the situation is somewhat similar to that encountered for the case of draining flow, as illustrated in Figure 8. In Figure 12, we present interface profiles at two different times, for that same case of a wide hole, with radius $\alpha = 4$. The Froude number $F = -0.1$ has the same magnitude as in Figure 8, although its sign is opposite, corresponding to injection rather than withdrawal.

Figure 12 shows that, for the wide hole with radius $\alpha = 4$, the interface forms a wave near the edge $r = \alpha$ of the injection hole. At later times, a packet of unstable waves then develops over the injection disk $r < \alpha$, and their amplitude increases with time. Eventually, the interface disturbance grows to the point that it intersects the plane at the top of the tank, and the solution ceases to be valid.

# 7   Conclusion and Discussion

In this paper, we have presented an analysis of the draining of a two-fluid system from a tank, for a model in which both fluids are assumed to be
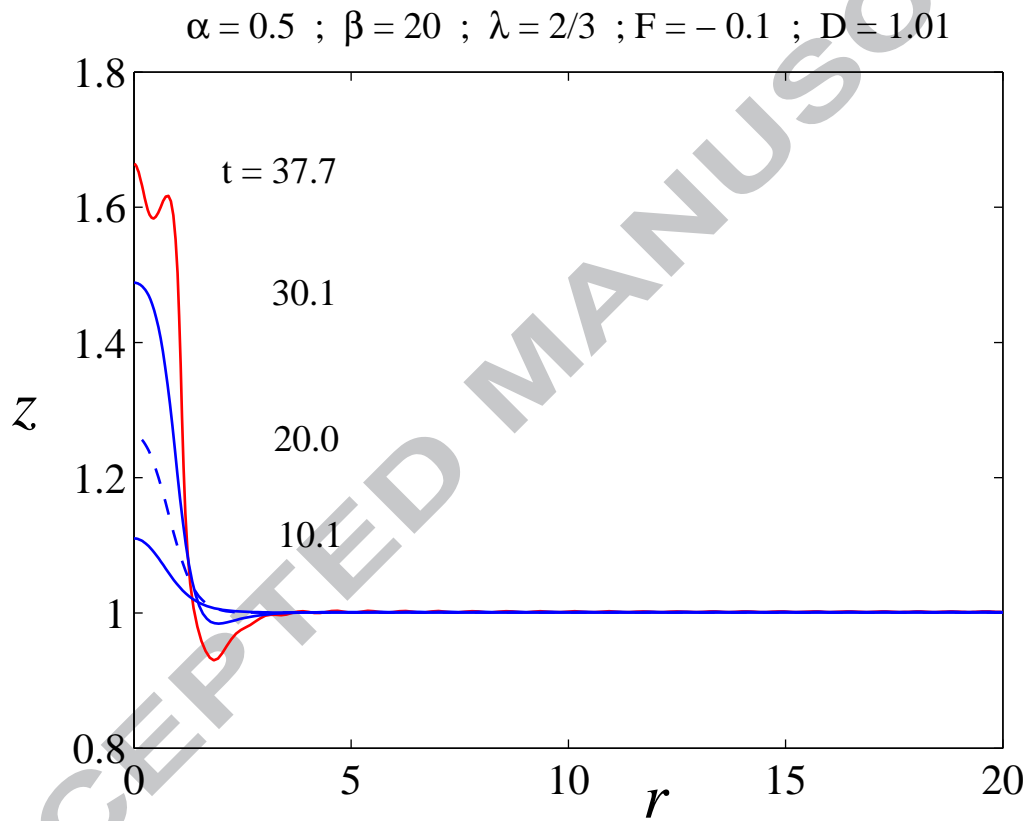
Figure 11: Four interface elevations for the unstable non-linear solution with density ratio $D = 0.99$ illustrated in Figure 9. The injection hole radius is $\alpha = 0.5$.
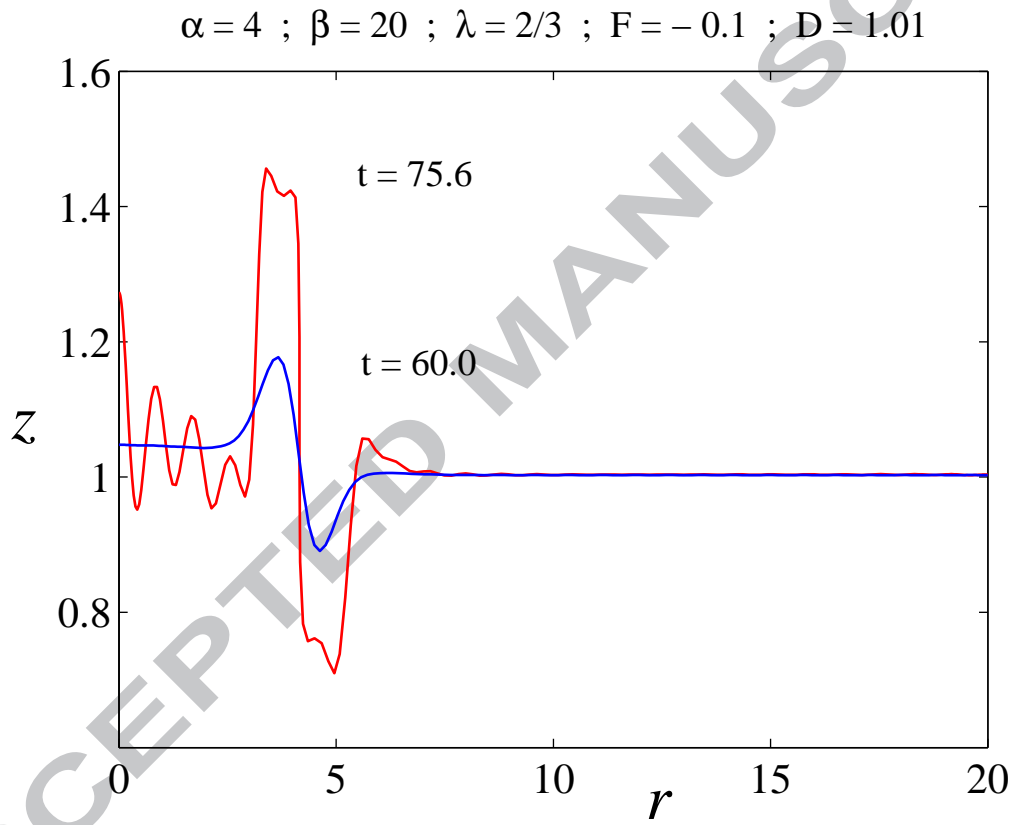
Figure 12: Two interface elevations for the unstable non-linear solution with density ratio $D = 1.01$, and wide injection hole radius $\alpha = 4$.

incompressible and inviscid, and there is a sharp interface between them. The flow is axially symmetric, so that the tank itself is a vertical cylinder with a hole in the bottom centred on the tank axis.

A linearized theory is available for this situation, and consists of small-amplitude variations about the draining flow in which the interface height simply drops uniformly according to the formula $\eta = 1 - (Ft)/(\pi\beta^2)$. For small Froude number $F$ or wide drain holes ($\alpha$ large), the linearized theory presented in section 3 gives an accurate account of the flow. It shows that waves at the interface reflect from the tank walls at $r = \beta$ and are focussed back toward the centre $r = 0$ where they are reflected back out again. This results in a pattern of relatively high-frequency oscillations experienced by the interface at the tank centre $r = 0$, as the overall interface level drops. These high-frequency disturbances are somewhat at odds with the corresponding two-dimensional (planar) draining flow, studied by Forbes and Hocking [16], in which the interfacial waves move much more slowly relative to the overall draining time required for the tank. This difference between the two flows is a consequence of the different geometries of the two situations, and the fact that, in the present cylindrically symmetric problem, there is a focussing effect of interfacial disturbances toward the centre.

An accurate and efficient method has been presented for the solution of the corresponding non-linear problem. The technique is based on a reasonably straightforward spectral representation of the solutions to Laplace's equations for the velocity potentials in each fluid layer, although it requires the use of Bessel functions of the first kind, and the use of the known recurrence relations for those functions (see ref. [20]). We have made use of the device introduced by Forbes *et al* [17], in which the interface is parametrized with a scaled arclength variable $\xi$. This allows for the possibility of the interface overturning and becoming multi-valued; this behaviour occurred even for the inviscid Rayleigh-Taylor type problem studied in [17] and was anticipated here, although it was not actually encountered. Nevertheless, different starting conditions for the drain could indeed lead to this behaviour in the present problem.

As with the two-dimensional problem studied by Forbes and Hocking [16], it has been found that there is good agreement between the predictions of the linearized approximation and the fully non-linear numerical results, during the early stages of the flow. Non-linear effects only become important when the interface level has dropped sufficiently close to the tank bottom, and it is found that the interface is then drawn rapidly into the drain hole. For narrow drain holes, in which $\alpha$ is small (this is broadly equivalent to the Froude number $F$ being large), a downwardly-directed vertical jet appears at the interface near the tank centre, and is then drawn uniformly into the

drain. For wider drains, in which $\alpha$ is large (or equivalently $F$ is very small), the interface draws down in a circular ring with radius roughly equal to that of the edge of the hole at $r = \alpha$. This results in an effective upwardly-directed jet at the centre $r = 0$ of the tank, consistent with the findings of Zhou and Graebel [13]. Similar (Froude number dependent) behaviour was also encountered by Stokes *et al* [12] in axially symmetric withdrawal flow, for fluid in an unbounded region.

In the two-dimensional equivalent of this problem, in which planar flow occurs as a result of withdrawal through a slot, Farrow and Hocking [15] computed solutions using an accurate finite-difference method, in the more general case in which some aspects of viscous behaviour were included and the interface was allowed to have finite thickness. They found that these additional effects mostly had only slight influence on the overall withdrawal flow, and this was supported by Forbes and Hocking [16] who were able to reproduce their results accurately using a purely inviscid model. Nevertheless, the results in the present paper suggest that the interface may develop regions of very high curvature toward the terminal stages of the withdrawal flow, and it is possible that viscosity could then trigger interface overhang and roll-up, as for the Kelvin-Helmholtz instability studied by Krasny [27], for example. We have briefly investigated the inclusion of surface-tension effects in this inviscid problem, as a possible way of regularizing the interface and potentially avoiding the appearance of large curvatures at the interface. For realistic values of the surface-tension parameter, however, no significantly different results were obtained. For planar inviscid flows, Moore [26] showed that curvature singularities could be generated at the interface within finite time; recent work by de la Hoz *et al* [32], however, indicates that surface tension may smooth this effect. Nevertheless, the curvature still grows rapidly in the presence of capillarity, so that interface roll-up could still be expected when viscosity is taken into account. This is supported by the work of Nie [33] which demonstrates that interfacial singularities of various types are possible in axially symmetric geometry even with the inclusion of surface tension.

In the present paper, we have also considered briefly the situation in which the upper fluid is heavier than the lower one, so that a type of Rayleigh-Taylor instability may result. The practical importance of such flows is possibly rather limited, and our initial interest in them was to see to what extent interface overturning might be possible in the presence of the background withdrawal or injection flow. It was found that instabilities developed rapidly at the interface, but that no inviscid roll-up or overhang was detected. Different initial conditions might nevertheless still produce this effect, however. The high curvature regions produced in such flows suggest that interface roll-up might indeed be encountered when viscous effects are re-introduced into the

35

model, and this awaits future work.

# 8 Appendix - Additional details of the Non-linear Solution Method

Fourier-Bessel decomposition of the arclength condition in section 4 gives rise to the system of differential equations (4.9), in which the intermediate variables are defined as the integral quantities

$$
\begin{aligned}
\mathcal{M}_{kn}(t) &= \int_0^\beta \xi \left( \frac{\partial r}{\partial \xi} \right) J_1' \left( j_{1,n} \frac{\xi}{\beta} \right) J_0 \left( j_{1,k} \frac{\xi}{\beta} \right) d\xi \\
\mathcal{N}_{kn}(t) &= \int_0^\beta \xi \left( \frac{\partial \eta}{\partial \xi} \right) J_1 \left( j_{1,n} \frac{\xi}{\beta} \right) J_0 \left( j_{1,k} \frac{\xi}{\beta} \right) d\xi.
\end{aligned} \tag{8.1}
$$

The zeroth-order Fourier mode in the first kinematic condition involves the intermediate integral quantities

$$
\begin{aligned}
\mathcal{H}_{0n} &= \int_0^\beta r \left( \frac{\partial \eta}{\partial \xi} \right) J_1 \left( j_{1,n} \frac{\xi}{\beta} \right) d\xi \\
\mathcal{R}_{0n} &= \int_0^\beta r \left( \frac{\partial r}{\partial \xi} \right) J_0 \left( j_{1,n} \frac{\xi}{\beta} \right) d\xi
\end{aligned} \tag{8.2}
$$

in the equation (4.15). The higher modes in the Fourier-Bessel decomposition of the first kinematic condition in equation (4.16) and the second condition in (4.17) both involve the further set

$$
\begin{aligned}
S_{kn}^{(1)}(t) &= \int_0^\beta r J_1 \left( j_{1,n} \frac{r}{\beta} \right) J_1 \left( j_{1,k} \frac{\xi}{\beta} \right) \sinh \left( j_{1,n} \frac{\eta}{\beta} \right) d\xi \\
S_{kn}^{(2)}(t) &= \int_0^\beta r J_1 \left( j_{1,n} \frac{r}{\beta} \right) J_1 \left( j_{1,k} \frac{\xi}{\beta} \right) \sinh \left( j_{1,n} \frac{(1+\lambda-\eta)}{\beta} \right) d\xi \\
T_{kn}^{(1)}(t) &= \int_0^\beta r J_0 \left( j_{1,k} \frac{\xi}{\beta} \right) \left[ \left( \frac{\partial \eta}{\partial \xi} \right) J_1 \left( j_{1,n} \frac{\xi}{\beta} \right) - \frac{2}{\beta^2} \left( \frac{\partial r}{\partial \xi} \right) \mathcal{H}_{0n} \right] d\xi \\
T_{kn}^{(2)}(t) &= \int_0^\beta r \left( \frac{\partial r}{\partial \xi} \right) J_0 \left( j_{1,k} \frac{\xi}{\beta} \right) \left[ J_0 \left( j_{1,n} \frac{\xi}{\beta} \right) - \frac{2}{\beta^2} \mathcal{R}_{0n} \right] d\xi
\end{aligned} \tag{8.3}
$$

of intermediate variables. In these expressions, $\mathcal{H}_{0n}$ and $\mathcal{R}_{0n}$ are as defined in equations (8.2). In addition, the differentiated form (4.18) of the second

36

kinematic condition makes use of the further sets of intermediate variables

$$
\begin{aligned}
K_{kn}(t) &= \int_0^\beta r J_1\left(j_{1,k}\frac{\xi}{\beta}\right)\left[J_1\left(j_{1,n}\frac{\xi}{\beta}\right)(W_2 - W_1) - \frac{2}{\beta^2}\mathcal{H}_{0n}(U_2 - U_1)\right] d\xi \\
L_{kn}(t) &= \int_0^\beta r J_1\left(j_{1,k}\frac{\xi}{\beta}\right)\left[J_0\left(j_{1,n}\frac{\xi}{\beta}\right) - \frac{2}{\beta^2}\mathcal{R}_{0n}\right](U_2 - U_1)\, d\xi, \qquad (8.4)
\end{aligned}
$$

which also involve the quantities in equation (8.2).

Finally, the zeroth and higher-order Fourier decomposition of the dynamic interfacial condition yields the systems of equations (4.20) and (4.21), in which the appropriate intermediate quantities are defined as

$$
\begin{aligned}
G_{kn}^{(1)}(t) &= \int_0^\beta \xi J_0\left(j_{1,n}\frac{r}{\beta}\right)J_0\left(j_{1,k}\frac{\xi}{\beta}\right)\cosh\left(j_{1,n}\frac{\eta}{\beta}\right) d\xi \\
G_{kn}^{(2)}(t) &= \int_0^\beta \xi J_0\left(j_{1,n}\frac{r}{\beta}\right)J_0\left(j_{1,k}\frac{\xi}{\beta}\right)\cosh\left(j_{1,n}\frac{(1+\lambda-\eta)}{\beta}\right) d\xi \\
J_k^{(1)}(t) &= \int_0^\beta \xi\left[\left(u^S + U_1\right)^2 + \left(w^S + W_1\right)^2\right]J_0\left(j_{1,k}\frac{\xi}{\beta}\right) d\xi \\
J_k^{(2)}(t) &= \int_0^\beta \xi\left[\left(u^S + U_2\right)^2 + \left(w^S + W_2\right)^2\right]J_0\left(j_{1,k}\frac{\xi}{\beta}\right) d\xi. \qquad (8.5)
\end{aligned}
$$

# References

[1] G.H. Jirka and D.S. Katavola, Supercritical withdrawal from two-layered fluid systems. Part 2: Three-dimensional flow into round intake, *J. Hyd. Res.*, **17** (1979) 53–62.

[2] I. Cohen, H. Li, J.L. Hougland, M. Mrksich and S.R. Nagel, Using selective withdrawal to coat microparticles, *Science*, **292** (2001) 265–267.

[3] D.H. Peregrine, A line source beneath a free surface, *Mathematics Research Center, Univ. Wisconsin Report*, **1248** (1972).

[4] E.O. Tuck and J.-M. Vanden-Broeck, A cusp-like free-surface flow due to a submerged source or sink, *J. Austral. Math. Soc., Ser. B*, **25** (1984) 443–450.

[5] T.E. Stokes, G.C. Hocking and L.K. Forbes, Unsteady free-surface flow induced by a line sink, *J. Eng. Math.*, **47** (2003) 137–160.

[6] L.K. Forbes, G.C. Hocking and T.E. Stokes, On starting conditions for a submerged sink in a fluid, *J. Eng. Math.*, (2008) to appear.

[7] L.K. Forbes and G.C. Hocking, Flow caused by a point sink in a fluid having a free surface, *J. Austral. Math. Soc., Ser. B*, **32** (1990) 231–249.

[8] L.K. Forbes and G.C. Hocking, Flow due to a sink near a vertical wall, in infinitely deep fluid, *Comput. Fluids*, **34** (2005) 684–704.

[9] T. Miloh and P.A. Tyvand, Nonlinear transient free-surface flow and dip formation due to a point sink, *Phys. Fluids Ser. A*, **5** (1993) 1368–1375.

[10] K.B. Haugen and P.A. Tyvand, Free-surface evolution due to an impulsive bottom sink at uniform depth, *Phys. Fluids*, **15** (2003) 742–751.

[11] M. Xue and D.K.P. Yue, Nonlinear free-surface flow due to an impulsively started submerged point sink, *J. Fluid Mech.*, **364** (1998) 325–347.

[12] T.E. Stokes, G.C. Hocking and L.K. Forbes, Unsteady flow induced by a withdrawal point beneath a free surface, *ANZIAM J.*, **47** (2005) 185–202.

[13] Q.-N. Zhou and W.P. Graebel, Axisymmetric draining of a cylindrical tank with a free surface, *J. Fluid Mech.*, **221** (1990) 511–532.

[14] J.H. Baek and H.Y. Chung, Numerical analysis on axisymmetric draining from a cylindrical tank with a free surface, *Comput. Fluid Dyn. J.*, **6** (1998) 413–425.

[15] D.E. Farrow and G.C. Hocking, A numerical model for withdrawal from a two-layer fluid, *J. Fluid Mech.*, **549** (2006) 141–157.

[16] L.K. Forbes and G.C. Hocking, Unsteady draining flows from a rectangular tank, *Phys. Fluids*, **19**, 082104 (2007) 14 pages.

[17] L.K. Forbes, M.J. Chen and C.E. Trenham, Computing unstable periodic waves at the interface of two inviscid fluids in uniform vertical flow, *J. Comput. Phys.*, **221** (2007) 269–287.

[18] M.-J. Kim, H.-T. Moon, Y.-B. Lee, S.-K. Choi, Y.-K. Kim, H.-Y. Nam and M. Cho, A spectral method for free surface flows of inviscid fluid, *Int. J. Numer. Meth. Fluids*, **28** (1998) 887–902.

38

[19] G.K. Batchelor, *An Introduction to Fluid Dynamics*. Cambridge University Press, Cambridge (1967).

[20] M. Abramowitz and I.A. Stegun, *A Handbook of Mathematical Functions*. Dover, New York (1972).

[21] J.A. Dutton, *The Ceaseless Wind: an introduction to the theory of atmospheric motion*. McGraw-Hill, Inc, New York (1976).

[22] G.K. Vallis, *Atmospheric and Oceanic Fluid Dynamics: fundamentals and large-scale circulation*. Cambridge University Press, Cambridge (2006).

[23] K.E. Atkinson, *An Introduction to Numerical Analysis*. Wiley, New York (1978).

[24] G. von Winckel, *lgwt.m*, at: MATLAB file exchange website, written (2004). `http://www.mathworks.com/matlabcentral/fileexchange/loadFile.do?objectId=4540&objectType=file`

[25] J.V. Wehausen and E.V. Laitone, *Surface Waves*, in: Encyclopaedia of Physics, **47** Springer Verlag, Berlin (1960). `http://www.coe.berkeley.edu/SurfaceWaves/`

[26] D.W. Moore, The spontaneous appearance of a singularity in the shape of an evolving vortex sheet, *Proc. R. Soc. Lond. A.*, **365** (1979) 105–119.

[27] R. Krasny, Desingularization of periodic vortex sheet roll-up, *J. Comput. Phys.*, **65** (1986) 292–313.

[28] G. Tryggvason, Numerical simulations of the Rayleigh-Taylor instability, *J. Comput. Phys.*, **75** (1988) 253–282.

[29] S. Chandrasekhar, *Hydrodynamic and Hydromagnetic Stability*. Dover, Inc., New York (1981).

[30] L.K. Forbes, Spectral solution methods for free-surface flow: the Rayleigh-Taylor problem, *ANZIAM J.*, **50** (2008) C549–C568. `http://anziamj.austms.org.au/ojs/index.php/ANZIAMJ/article/viewFile/1393/1197`

[31] L.K. Forbes, The Rayleigh-Taylor instability for inviscid and viscous fluids, *J. Eng. Math.*, **65** (2009) 273–290.

[32] F. de la Hoz, M.A. Fontelos and L. Vega, The effects of surface tension on the Moore singularity of vortex sheet dynamics, *J. Nonlinear Sci.*, **18** (2008) 463–484.

[33] Q. Nie, The nonlinear evolution of vortex sheets with surface tension in axisymmetric flows, *J. Comput. Phys.*, **174** (2001) 438–459.